Numerical study of the KP equation for non-periodic waves

Chiu-Yen Kao† and Yuji Kodama*

Department of Mathematics, The Ohio State University, Columbus, OH 43210

arXiv:1004.0407v1 [nlin.PS] 3 Apr 2010

Abstract

The Kadomtsev-Petviashvili (KP) equation describes weakly dispersive and small amplitude waves propagating in a quasi-two dimensional situation. Recently a large variety of exact soliton solutions of the KP equation has been found and classified. Those soliton solutions are localized along certain lines in a two-dimensional plane and decay exponentially everywhere else, and they are called line-soliton solutions in this paper. The classification is based on the far-field patterns of the solutions which consist of a finite number of line-solitons. In this paper, we study the initial value problem of the KP equation with V- and X-shape initial waves consisting of two distinct line-solitons by means of the direct numerical simulation. We then show that the solution converges asymptotically to some of those exact soliton solutions. The convergence is in a locally defined L^2-sense. The initial wave patterns considered in this paper are related to the rogue waves generated by nonlinear wave interactions in shallow water wave problem.

Keywords: Kadomtsev-Petviashvili equation, soliton solutions, chord diagrams, pseudo-spectral method, window technique

1. Introduction

The KdV equation may be obtained in the leading order approximation of an asymptotic perturbation theory for one-dimensional nonlinear waves under the assumptions of weak nonlinearity (small amplitude) and weak dispersion (long waves). The initial value problem of the KdV equation has been extensively studied by means of the method of inverse scattering transform (IST). It is then well-known that a general initial data decaying rapidly for large spatial variable evolves into a sum of individual solitons and some weak dispersive wave trains separated away from solitons (see for examples, [1, 13, 15, 20]).

In 1970, Kadomtsev and Petviashvili [7] proposed a two-dimensional dispersive wave equation to study the stability of one soliton solution of the KdV equation under the influence of weak transversal perturbations. This equation is now referred to as the KP equation, and considered to be a prototype of the integrable nonlinear dispersive wave equations in two dimensions. The KP equation can be also represented in the Lax form, that is, there exists a pair of linear equations associated with the eigenvalue problem and the evolution of the eigenfunctions. However, unlike the case of the KdV equation, the method of IST based on the pair of linear equations does not seem to provide a practical method for the initial value problem with non-periodic waves considered in this paper. At the present time, there is no feasible analytic method to solve the initial value problem of the KP equation with initial waves having line-solitons in the far field.

In this paper, we study this type of the initial value problem of the KP equation by means of the direct numerical simulation. In particular, we consider the following two cases of the initial waves: In the first case, the initial wave consists of two semi-infinite line-solitons forming a V-shape pattern, and in the second case, the initial wave is given by a linear combination of two infinite line-solitons forming X-shape. Those initial waves have been considered in the study of the generation of large amplitude waves in shallow water [16, 18, 10]. The main result of this paper is to show that the solutions of the initial value problem with those initial waves asymptotically *converge* to some of the exact soliton solutions found in [2, 3]. This implies a separation of the (exact) soliton solution from the dispersive radiations in the similar manner as in the KdV case.

The paper is organized as follows: In Section 2, we provide a brief summary of the soliton solutions of the KP equation and the classification theorem obtained in [2, 3] for those soliton solutions as a background necessary for the present study. In particular, we introduce the parametrization of each soliton solution with a *chord diagram* which represents a derangement of the permutation group, i.e. permutation without fixed point. In Section 3, we present several exact soliton solutions, and describe some properties of those solutions. Each of those soliton solutions has N_+ numbers of line-solitons in a far field on the two-dimensional plane, say in $y \gg 0$, and N_- numbers of line-solitons in the far field of the opposite side, i.e. $y \ll 0$. This type of soliton solution is referred to as an (N_-, N_+)-soliton solution. Here we consider those solitons with $N_- + N_+ \leq 4$ and $N_- \leq 3$. In Section 4, we describe the numerical scheme used in this paper, which is based on the pseudo-spectral method combined with the window technique [17, 19]. The window technique is especially used to compute our non-periodic problem which is essentially an infinite domain problem. Finally, in Section 5, we present the numerical results of the initial value problems with V- and X-shape initial waves, and show that the solutions asymptotically converge to some of those exact solutions discussed in Section 3. The convergence is in the sense of locally defined L_2-sense with the usual norm, i.e. $\|f\|_{L^2(D)} := \left(\iint_D |f(x,y)|^2 dxdy\right)^{\frac{1}{2}}$, where $D \subset \mathbb{R}^2$ is a compact set which covers the main structure describing the (resonant) interactions in the solution. We also propose a method to identify an exact solution for a given initial wave with V- or X-shape pattern based on the chord diagrams introduced in the classification theory.

2. Background

Here we give a brief summary of the recent result of the classification theorem for soliton solutions of the KP equation (see [9, 2, 3] for the details). In particular, each soliton solution is then parametrized by a chord diagram which represents a unique element of the permutation group. We use this parametrization throughout the paper.

2.1. The KP equation

The KP equation is a two-dimensional nonlinear dispersive wave equation given by

$$\partial_x \left(4\partial_t u + 6u\partial_x u + \partial_x^3 u\right) + 3\partial_y^2 u = 0, \tag{2.1}$$

where $\partial_x^n u := \dfrac{\partial^n u}{\partial x^n}$ etc. Let us express the solution in the form,

$$u(x,y,t) = 2\,\partial_x^2 \ln \tau(x,y,t)\,. \tag{2.2}$$

where the function τ is called the *tau* function, which plays a central role in the KP theory. In this paper, we consider a class of the solutions, where each solution can be expressed by $\tau(x,y,t)$ in the Wronskian determinant form $\tau = \mathrm{Wr}(f_1, \ldots, f_N)$, i.e.

$$\tau(x,y,t) = \begin{vmatrix} f_1 & f_1' & \cdots & f_1^{(N-1)} \\ f_2 & f_2' & \cdots & f_2^{(N-1)} \\ \vdots & \vdots & \ddots & \vdots \\ f_N & f_N' & \cdots & f_N^{(N-1)} \end{vmatrix}, \tag{2.3}$$

with $f_n^{(j)} := \partial_x^j f_n$ for $n = 1, \ldots, N$. Here the functions $\{f_1, \ldots, f_N\}$ form a set of linearly independent solutions of the linear equations,

$$\partial_y f_n = \partial_x^2 f_n, \qquad \partial_t f_n = -\partial_x^3 f_n.$$

(The fact that (2.2) with (2.3) gives a solution of the KP equation is well-known and the proof can be found in several places, e.g. see [6, 3].) The solution of those equations can be expressed in the Fourier transform,

$$f_n(x,y,t) = \int_C e^{kx+k^2y-k^3t}\,\rho_n(k)\,dk\,, \qquad n = 1, 2, \ldots, N, \tag{2.4}$$

with an appropriate contour C in $\mathbb{C}$ and the measure $\rho_n(k)\,dk$. In particular, we consider a finite dimensional solution with $\rho_n(k)\,dk = \sum_{m=1}^{M} a_{n,m}\delta(k-k_m)\,dk$ with $a_{n,m} \in \mathbb{R}$, i.e.

$$f_n(x,y,t) = \sum_{m=1}^{M} a_{n,m}E_m(x,y,t) \qquad \text{with} \quad E_m = \exp(k_m x + k_m^2 y - k_m^3 t).$$

Thus this type of solution is characterized by the parameters $\{k_1, k_2, \ldots, k_M\}$ and the $N \times M$ matrix $A := (a_{n,m})$ of $\mathrm{rank}(A) = N$, that is, we have

$$(f_1, f_2, \ldots, f_N) = (E_1, E_2, \ldots, E_M)A^T\,. \tag{2.5}$$

Note that $\{E_1, E_2, \ldots, E_M\}$ gives a basis of $\mathbb{R}^M$ and $\{f_1, f_2, \ldots, f_N\}$ spans an N-dimensional subspace of $\mathbb{R}^M$. This means that the A-matrix can be identified as a point on the real Grassmann manifold $\mathrm{Gr}(N, M)$ (see [9, 3]). More precisely, let $M_{N\times M}(\mathbb{R})$ be the set of all $N \times M$ matrices of rank N. Then $\mathrm{Gr}(N, M)$ can be expressed as

$$\mathrm{Gr}(N, M) = \mathrm{GL}_N(\mathbb{R})\backslash M_{N\times M}(\mathbb{R}),$$

where $\mathrm{GL}_N(\mathbb{R})$ is the general linear group of rank N. This is saying that other basis $(g_1, \ldots, g_N) = (f_1, \ldots, f_N)H$ for any $H \in \mathrm{GL}_N(\mathbb{R})$ spans the same subspace. Notice here that the freedom in the A-matrix with $\mathrm{GL}_N(\mathbb{R})$ can be fixed by expressing A in the reduced row echelon form (RREF). We then assume throughout this paper that the A-matrix is in the RREF, and show that the A-matrix plays a crucial role in our discussion on the asymptotic behavior of the initial value problem.

Now using the Binet-Cauchy Lemma for the determinant, the τ-function of (2.2) can be expressed in the form,

$$\begin{aligned}\tau &= \left|\begin{pmatrix} E_1 & E_2 & \cdots & \cdots & E_M \\ k_1E_1 & k_2E_2 & \cdots & \cdots & k_ME_M \\ \vdots & \vdots & \ddots & \ddots & \vdots \\ k_1^{N-1}E_1 & k_2^{N-1}E_2 & \cdots & \cdots & k_M^{N-1}E_M \end{pmatrix}\begin{pmatrix} a_{11} & a_{21} & \cdots & a_{N1} \\ a_{12} & a_{22} & \cdots & a_{N2} \\ \vdots & \vdots & \ddots & \vdots \\ \vdots & \vdots & \ddots & \vdots \\ a_{1M} & a_{2M} & \cdots & a_{NM} \end{pmatrix}\right| \\ &= \sum_{1\le j_1<j_2<\cdots<j_N\le M} \xi(j_1, j_2, \ldots, j_N)E(j_1, j_2, \ldots, E_N),\end{aligned} \tag{2.6}$$

where $\xi(j_1, \ldots, j_N)$ is the $N \times N$ minor of the A-matrix with N columns marked by $(j_1, \ldots, j_N)$, and $E(j_1, \ldots, j_N)$ is given by

$$E(j_1, \ldots, j_N) = \mathrm{Wr}(E_{j_1}, \ldots, E_{j_N}) = \prod_{l<m}(k_{j_m} - k_{j_l})E_{j_1}\cdots E_{j_N}.$$

From the formula (2.6), one can see that for a given A-matrix,

- if a column of A has only zero elements, then the exponential term E_m with m being the column index never appear in the τ-function, and
- if a row of A has only the pivot as non-zero element, then E_n with n being the row index can be factored out from the τ-function, i.e. E_n has no contribution to the solution.

We then say that an A-matrix with no such cases is *irreducible*, because the τ-function with reducible matrix can be obtained by a matrix with smaller size.

We are also interested in non-singular solutions. Since the solution is given by $u = 2\partial_x^2(\ln\tau)$, the non-singular solutions are obtained by imposing the non-negativity condition on the minors,

$$\xi(j_1, j_2, \ldots, j_N) \ge 0, \qquad \text{for all} \quad 1 \le j_1 < j_2 < \cdots < j_N \le M. \tag{2.7}$$

This condition is not only sufficient but also necessary for the non-singularity of the solution. We call a matrix having the condition (2.7) *totally non-negative* matrix.

2.2. Line-soliton solution and the notations

Let us here present the simplest solution, called one *line-soliton* solution, and introduce several notations to describe the solution. A line-soliton solution is obtained by a τ-function with two exponential terms, i.e. the case $N = 1$ and $M = 2$ in (2.5): With the A-matrix of the form $A = (1\ a)$, we have

$$\tau = E_1 + aE_2 = 2\sqrt{a}e^{\frac{1}{2}(\theta_1+\theta_2)}\cosh\frac{1}{2}(\theta_1 - \theta_2 - \ln a)\,,$$

The parameter a in the A-matrix must be $a \geq 0$ for a *non-singular* solution (i.e. totally non-negative A-matrix), and it determines the location of the soliton solution. Since $a = 0$ leads to a trivial solution, we consider only $a > 0$ (i.e. irreducible A-matrix) . Then the solution $u = 2\partial_x^2(\ln\tau)$ gives

$$u = \frac{1}{2}(k_1 - k_2)^2\,\mathrm{sech}^2\,\frac{1}{2}(\theta_1 - \theta_2 - \ln a).$$

Thus the solution is located along the line $\theta_1 - \theta_2 = \ln a$. We here emphasize that the line-soliton appears at the boundary of two regions, in each of which either E_1 or E_2 becomes the dominant exponential term, and because of this we also call this soliton $[1, 2]$-soliton solution (or soliton of $[1, 2]$-type). In general, the line-soliton solution of $[i, j]$-type with $i < j$ has the following structure (sometimes we consider only locally),

$$u = A_{[i,j]}\,\mathrm{sech}^2\,\frac{1}{2}\left(\mathbf{K}_{[i,j]}\cdot\mathbf{x} - \Omega_{[i,j]}t + \Theta_{[i,j]}\right) \tag{2.8}$$

with some constant $\Theta_{[i,j]}$. The amplitude $A_{[i,j]}$, the wave-vector $\mathbf{K}_{[i,j]}$ and the frequency $\Omega_{[i,j]}$ are defined by

$$\begin{aligned}
A_{[i,j]} &= \frac{1}{2}(k_j - k_i)^2\\
\mathbf{K}_{[i,j]} &= \left(k_j - k_i, k_j^2 - k_i^2\right) = (k_j - k_i)\left(1, k_i + k_j\right),\\
\Omega_{[i,j]} &= k_j^3 - k_i^3 = (k_j - k_i)(k_i^2 + k_ik_j + k_j^2).
\end{aligned}$$

The direction of the wave-vector $\mathbf{K}_{[i,j]} = (K^x_{[i,j]}, K^y_{[i,j]})$ is measured in the counterclockwise from the x-axis, and it is given by

$$\frac{K^y_{[i,j]}}{K^x_{[i,j]}} = \tan\Psi_{[i,j]} = k_i + k_j.$$

Notice that $\Psi_{[i,j]}$ gives the angle between the line $\mathbf{K}_{[i,j]}\cdot\mathbf{x} = const$ and the y-axis (See Figure 2.1). Then a line-soliton (2.8) can be written in the form with three parameters $A_{[i,j]}$, $\Psi_{[i,j]}$ and $x^0_{[i,j]}$,

$$u = A_{[i,j]}\,\mathrm{sech}^2\,\sqrt{\frac{A_{[i,j]}}{2}}\left(x + y\tan\Psi_{[i,j]} - C_{[i,j]}t - x^0_{[i,j]}\right), \tag{2.9}$$

with $C_{[i,j]} = k_i^2 + k_ik_j + k_j^2 = \frac{1}{2}A_{[i,j]} + \frac{3}{4}\tan^2\Psi_{[i,j]}$. For the parameter $x^0_{[i,j]}$ giving the location of the line-soliton, we also use the notation,

$$x^0_{[i,j]} = -\frac{1}{k_j - k_i}\Theta_{[i,j]}, \tag{2.10}$$

with $\Theta_{[i,j]}$ in (2.8) which is determined by the A-matrix and the k-parameters. For multi-soliton solutions, one can only define the location of each $[i, j]$-soliton using the asymptotic position in the xy-plane either $x \gg 0$ or $x \ll 0$ (we mainly consider the cases where the solitons are not parallel to the y-axis), and we use the notation $x^+_{[i,j]}$ (or $x^-_{[i,j]}$) which describes the *x-intercept* of the line determined by the wave crest of $[i, j]$-soliton in the region $x \gg 0$ (or $x \ll 0$) at $t = 0$. In Figure 2.1, we illustrate an example of one line-soliton solution. In the right panel of this figure, we show a *chord diagram* which represents this soliton solution. Here the chord diagram indicates the permutation of the dominant exponential terms E_i and E_j in the τ-function, that is, with the ordering $k_i < k_j$, E_i dominates in $x \ll 0$, while E_j dominates in $x \gg 0$. This representation of the line-solitons in terms of the chord diagrams is the key concept throughout the present paper. (See section 2.3 below for the precise definition of the chord diagrams.)

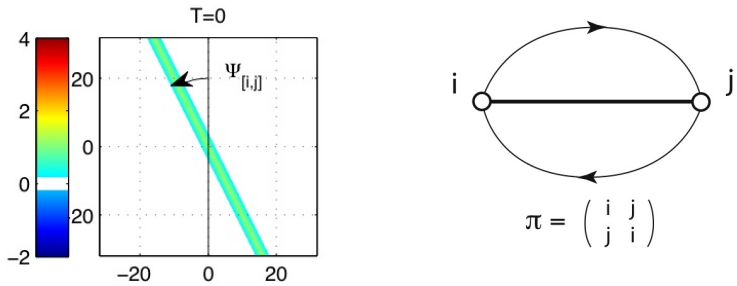

Figure 2.1: One line-soliton solution of $[i, j]$-type and the corresponding chord diagram. The amplitude $A_{[i,j]}$ and the angle $\Psi_{[i,j]}$ are given by $A_{[i,j]} = \frac{1}{2}(k_i - k_j)^2$ and $\tan\Psi_{[i,j]} = k_i + k_j$. The upper oriented chord represents the part of $[i, j]$-soliton for $y \gg 0$ and the lower one for $y \ll 0$. Here i, j represent not just k_i, k_j, but also the value of those parameters, i.e. the horizontal line is the coordinate for the k-parameters, and in this example, $k_1 = -0.5$ and $k_2 = 1$.

For each soliton solution of (2.9), the wave vector $\mathbf{K}_{[i,j]}$ and the frequency $\Omega_{[i,j]}$ satisfy the soliton-dispersion relation, i.e.,

$$4\Omega_{[i,j]}K^x_{[i,j]} = (K^x_{[i,j]})^4 + 3(K^y_{[i,j]})^2. \tag{2.11}$$

The soliton velocity $\mathbf{V}_{[i,j]}$ defined by $\mathbf{K}_{[i,j]} \cdot \mathbf{V}_{[i,j]} = \Omega_{[i,j]}$ is given by

$$\mathbf{V}_{[i,j]} = \frac{\Omega_{[i,j]}}{|\mathbf{K}_{[i,j]}|^2}\mathbf{K}_{[i,j]} = \frac{k_i^2 + k_ik_j + k_j^2}{1 + (k_i + k_j)^2}\,(1,\ k_i + k_j).$$

Note in particular that $C_{[i,j]} = k_i^2 + k_ik_j + k_j^2 > 0$, and this implies that the x-component of the velocity is *always* positive, that is, any soliton propagates in the positive x-direction. On the other hand, one should note that any small perturbation propagates in the negative x-direction, that is, the x-component of the group velocity is always negative. This can be seen from the dispersion relation of the KP equation for a linear wave $\phi = \exp(i\mathbf{k} \cdot \mathbf{x} - i\omega t)$ with the wave-vector $\mathbf{k} = (k_x, k_y)$ and the frequency ω,

$$\omega = -\frac{1}{4}k_x^3 + \frac{3}{4}\frac{k_y^2}{k_x},$$

from which the group velocity of the wave is given by

$$\mathbf{v} = \nabla\omega = \left(\frac{\partial\omega}{\partial k_x}, \frac{\partial\omega}{\partial k_y}\right) = \left(-\frac{3}{4}\left(k_x^2 + \frac{k_y^2}{k_x^2}\right), \frac{2}{3}\frac{k_y}{k_x}\right).$$

This is similar to the case of the KdV equation, and we expect that asymptotically soliton separates from small radiations. Physically this implies that soliton is a *supersonic* wave due to its nonlinearity (recall that the velocity of shallow water wave is proportional to the square root of the water depth, and the KP equation in the form (2.1) describes the waves in the moving frame with the phase velocity in the x-direction).

Stability of one-soliton solution was shown in the original paper by Kadomtsev and Petviashvii [7], and this may be stated as follows: For any $\epsilon > 0$ and any $r > 0$, there exists $\delta > 0$ so that if the initial wave $u(x, y, 0) := u^0(x, y)$ satisfies

$$\|u^0 - u^0_{\text{exact}}\|_{L^2(D^0_r)} < \delta,$$

for some exact soliton solution, $u^t_{\text{exact}} := A_0 \operatorname{sech}^2 \sqrt{\frac{A_0}{2}}(x + y\tan\Psi_0 - C_0t - x_0)$ with appropriate constants A_0, Ψ_0 and x_0 (recall $C_0 = \frac{1}{2}A_0 + \frac{3}{4}\tan^2\Psi_0$), then the stability implies that the solution $u^t(x, y) := u(x, y, t)$ satisfies

$$\|u^t - u^t_{\text{exact}}\|_{L^2(D^t_r)} < \epsilon, \quad \text{for} \quad t \to \infty,$$

where D^t_r is a circular disc with radius r moving with the soliton, i.e.

$$D^t_r = \{(x, y) \in \mathbb{R}^2 : (x - x_0(t))^2 + (y - y_0(t))^2 \le r^2\},$$

with $(x_0(t), y_0(t))$ at any point on the soliton, $x_0(t) + y_0(t)\tan\Psi_0 = C_0 t + x_0$. Here $\|f\|_{L^2(D)}$ is the usual L^2-norm of $f(x, y)$ over a compact domain $D \subset \mathbb{R}^2$, i.e.

$$\|f\|_{L^2(D)} := \left(\iint_D |f(x, y)|^2 \, dxdy \right)^{\frac{1}{2}}.$$

This stability implies a separation of the soliton from the dispersive radiations (non-soliton parts) as in the case of the KdV soliton. We would like to prove the similar statement for more general initial waves. However there are several difficulties for two-dimensional stability problem in general. In this paper, we will give a numerical study for some special cases where the initial waves consist of two semi-infinite line solitons with V- or X-shape.

Finally we remark that a line-soliton having the angle $\Psi \approx \frac{\pi}{2}$ has an infinite speed, and of course it is beyond the assumption of the quasi-two dimensionality. We also emphasize that the structure of the solution for $y \gg 0$ can be different from that in $y \ll 0$, that is, the set of asymptotic solitons in $y \gg 0$ can be different from that in $y \ll 0$. This difference is a consequence of the resonant interactions among solitons as we can see throughout the paper.

2.3. Classification Theorems

Now we present the main theorems obtained in [2, 3] for the classification of soliton solutions generated by the τ-functions with irreducible and totally non-negative A-matrices:

Theorem 2.1. *Let $\{e_1, \ldots, e_N\}$ be the pivot indices, and let $\{g_1, \ldots, g_{M-N}\}$ be non-pivot indices for an $N \times M$ irreducible and totally non-negative A-matrix. Then the soliton solution generated by the τ-function with the A-matrix has the following asymptotic structure:*

(a) For $y \gg 0$, there are N line-solitons of $[e_n, j_n]$-type for $n = 1, \ldots, N$.

(b) For $y \ll 0$, there are $M - N$ line-solitons of $[i_m, g_m]$-type for $m = 1, \ldots, M - N$.

Here $j_n (> e_n)$ and $i_m (< g_m)$ are determined uniquely from the A-matrix.

The unique index pairings $[e_n, j_n]$ and $[i_m, g_m]$ in Theorem 2.1 have a combinatorial interpretation. Let us define the pairing map $\pi : \{1, 2, \ldots, M\} \to \{1, 2, \ldots, M\}$ such that

$$\begin{cases} \pi(e_n) = j_n, & n = 1, \ldots, N, \\ \pi(g_m) = i_m, & m = 1, \ldots, M - N, \end{cases} \tag{2.12}$$

where e_n and g_m are respectively the pivot and non-pivot indices of the A-matrix. Then we have:

Theorem 2.2. *The pairing map π is a bijection. That is, $\pi \in S_M$, where S_M is the group of permutation for the index set $\{1, 2, \ldots, M\}$, i.e.*

$$\pi = \begin{pmatrix} e_1 & \cdots & e_N & g_1 & \cdots & g_{M-N} \\ j_1 & \cdots & j_N & i_1 & \cdots & i_{M-N} \end{pmatrix}$$

Note in particular that the corresponding π is the derangement, i.e. π has no fixed point.

Theorem 2.2 shows that the pairing map π for an $(M - N, N)$-soliton solution has N *excedances*, i.e. $\pi(i) > i$ for $i = 1, \ldots, N$, and the excedance set is the set of pivot indices of the A-matrix. We represent each soliton solution with the *chord diagram* defined as follows:

(i) There are M marked points on a line, each of the point corresponds to the k-parameter.

(ii) On the upper side of the line, there are N chords (pairings), each of them connects two points on the line representing $\pi(e_n) = j_n$ for $n = 1, \ldots, N$, i.e. the excedance $j_n > e_n$.

(iii) On the lower side of the line, there are $M - N$ chords representing $\pi(g_m) = i_m$ for $m = 1, \ldots, M - N$, i.e. the deficiency $i_m < g_m$.

In Figure 2.2, we illustrate an example of the chord diagram which represents the derangement,

$$\pi = \begin{pmatrix} 1 & 2 & 3 & 4 & 5 & 6 & 7 & 8 \\ 4 & 6 & 5 & 2 & 3 & 8 & 1 & 7 \end{pmatrix} \quad \text{or simply} \quad \pi = (46523817).$$

The diagram then shows that the set of excedances is $\{1, 2, 3, 6\}$, and the corresponding soliton solution consists of the asymptotic line-solutions of $[1, 4]$-, $[2, 6]$-, $[3, 5]$- and $[6, 8]$-types in $y \gg 0$ and of $[1, 7]$-, $[2, 4]$-, $[3, 5]$- and $[7, 8]$-types in $y \ll 0$.

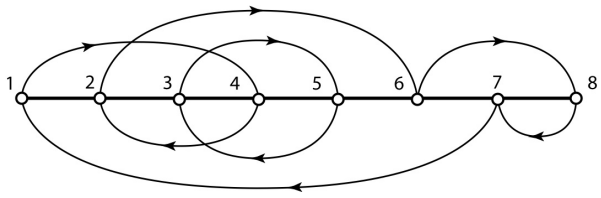

Figure 2.2: Example of the chord diagram. This shows $\pi = (46523817)$. Each chord joining i-th and j-th marked points represents the line-soliton of $[i, j]$-type.

3. Exact solutions

Here we present several exact solutions generated by smaller size matrices with $N \leq 3$ and $M \leq 4$. Those solutions give a fundamental structure of general solutions, and we will show that some of those solutions appear naturally as asymptotic solutions of the KP equation for certain classes of initial waves related to the rogue wave generation [16, 18, 19, 5]. The detailed discussions and the formulae given in this section can be found in [3].

3.1. Y-shape solitons: Resonant solutions

We first discuss the resonant interaction among line-solitons, which is the most important feature of the KP equation (see e.g. [11, 14, 8]). To describe resonant solutions, let us consider the τ-function with $M = 3$, that is, the τ-function has three exponential terms $\{E_1, E_2, E_3\}$. In terms of the τ-function in the form (2.3), those are given by the cases $(N = 1, M = 3)$ and $(N = 2, M = 3)$.

Let us first study the case with $N = 1$ and $M = 3$, where the A-matrix is given by

$$A = \begin{pmatrix} 1 & a & b \end{pmatrix}.$$

The parameters a, b in the matrix are positive constants, and the positivity implies the irreducibility and the regularity of the solution. The τ-function is simply given by

$$\tau = E_1 + aE_2 + bE_3.$$

(Note that if one of the parameters is zero, then the τ-function consists only two exponential terms and it gives one line-soliton solution, i.e. reducible case.) With the ordering $k_1 < k_2 < k_3$, the solution $u = 2\partial_x^2(\ln \tau)$ consists of $[1, 3]$-soliton for $y \gg 0$ and $[1, 2]$- and $[2, 3]$-solitons for $y \ll 0$. Taking the balance between two exponential terms in the τ-function, one can see that those line-solitons of $[1, 3]$- and $[2, 3]$-types are localized along the lines given in (2.9), i.e. $x + y \tan \Psi_{[i,j]} - C_{[i,j]}t = x^0_{[i,j]}$ for $[i, j] = [1, 3]$ and $[2, 3]$ where the locations $x^0_{[i,j]}$ are determined by the A-matrix (see (2.10)),

$$x^0_{[1,3]} = -\frac{1}{|3, 1|} \ln b, \qquad x^0_{[2,3]} = -\frac{1}{|3, 2|} \ln \frac{b}{a}. \tag{3.1}$$

where $|i, j| := k_i - k_j$. The shape of solution generated by $\tau = E_1 + aE_2 + bE_3$ with $a = b = 1$ (i.e. at $t = 0$ three line-solitons meet at the origin) is illustrated via the contour plot in the first row of Figure 3.1. This solution represents a resonant solution of three line-solitons, and the resonant condition is given by

$$\mathbf{K}_{[1,3]} = \mathbf{K}_{[1,2]} + \mathbf{K}_{[2,3]}, \qquad \Omega_{[1,3]} = \Omega_{[1,2]} + \Omega_{[2,3]},$$

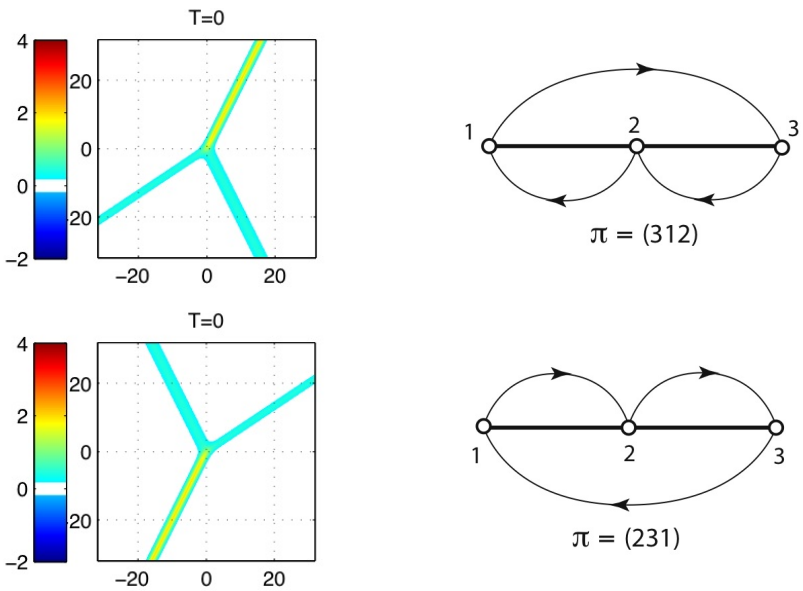

Figure 3.1: Examples of $(2,1)$- and $(1,2)$-soliton solutions and the chord diagrams. The k-parameters are given by $(k_1, k_2, k_3) = (-\frac{5}{4}, -\frac{1}{4}, \frac{3}{4})$. The right panels are the corresponding chord diagrams. For both cases, the parameters in the A-matrices are chosen so that at $t = 0$ three line-solitons meet at the origin as shown in the left panels.

which are trivially satisfied with $\mathbf{K}_{[i,j]} = (k_j - k_i, k_j^2 - k_i^2)$ and $\Omega_{[i,j]} = k_j^3 - k_i^3$. The chord diagram corresponding to this soliton is shown in the right panel of the first raw in Figure 3.1, and it represents the permutation $\pi = (312)$.

Let us now consider the case with $N = 2$ and $M = 3$: We take the A-matrix in the form,

$$A = \begin{pmatrix} 1 & 0 & -b \\ 0 & 1 & a \end{pmatrix}.$$

where a and b are positive constants. Then the τ-function is given by

$$\tau = E(1,2) + aE(1,3) + bE(2,3),$$

with $E(i,j) = (k_j - k_i)E_iE_j$ for $i < j$. In this case we have $[1,2]$- and $[2,3]$-solitons for $y \gg 0$ and $[1,3]$-soliton for $y \ll 0$, and this solution can be labeled by $\pi = (231)$. Those line-solitons of $[1,2]$- and $[1,3]$-types are localized along the lines, $x + y\tan\Psi_{[i,j]} - C_{[i,j]}t = x^0_{[i,j]}$ with

$$x^0_{[1,2]} = -\frac{1}{|2,1|}\ln\left(\frac{|3,2|}{|3,1|}\frac{b}{a}\right), \qquad x^0_{[1,3]} = -\frac{1}{|3,1|}\ln\left(\frac{|3,2|}{|2,1|}b\right), \tag{3.2}$$

where $|i,j| := k_i - k_j$. In the lower figures of Figure 3.1, we illustrate the solution in this case. Notice that this figure can be obtained from $(2,1)$-soliton in the upper figure by changing $(x,y) \to (-x,-y)$. Here the parameters a and b in the A-matrix are chosen, so that $x^0_{[1,2]} = x^0_{[1,3]} = 0$, that is, all of those soliton solutions meet at the origin at $t = 0$.

3.2. $N = 1, 3$ *and* $M = 4$ *cases*

Let us first discuss the case with $N = 1$ and $M = 4$, that is, the A-matrix is given by

$$A = (1\ a\ b\ c),$$

where a, b and c are positive constants. The τ-function is simply written in the form

$$\tau = E_1 + aE_2 + bE_3 + cE_4.$$

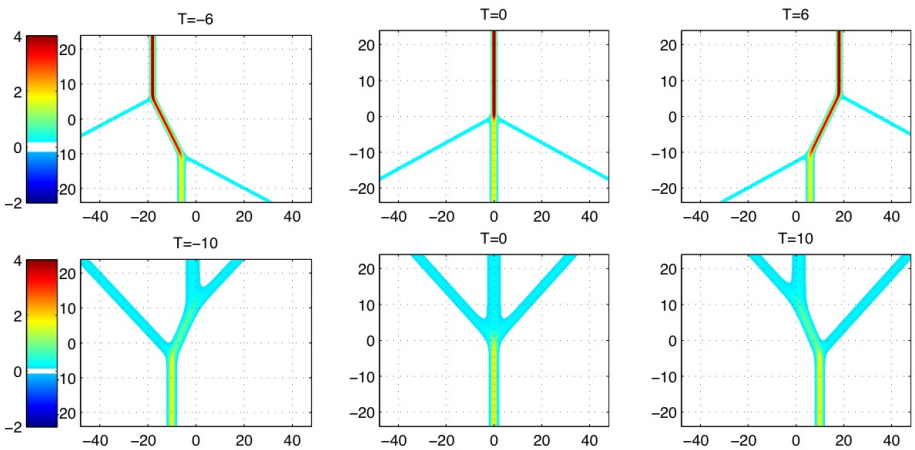

Figure 3.2: Examples of $(3,1)$- and $(1,3)$-soliton solutions. The solution in the upper figures are generated by the 1×4 A-matrix with $(k_1,k_2,k_3,k_4)=(-\sqrt{3},-1,1,\sqrt{3})$. The symmetry in the k-parameters implies that $[1,4]$- and $[2,3]$-solitons are parallel to the y-axis. The lower figures are generated by the 3×4 A-matrix with $(k_1,k_2,k_3,k_4)=(-1,-\frac{1}{2\sqrt{2}},\frac{1}{2\sqrt{2}},1)$.

In this case, we have $(3,1)$-soliton solution consisting of one line-soliton of $[1,4]$-type for $y\gg 0$ and three line-solitons of $[1,2]$-, $[2,3]$- and $[3,4]$-types for $y\ll 0$. This solution is labeled by $\pi=(4\,1\,2\,3)$. The upper figures in Figure 3.2 shows the time-evolution of the solution of this type. We set $a=b=c=1$ of the A-matrix, so that all four line-solitons meet at the origin at $t=0$.

For $N=3$, any irreducible and totally non-negative A-matrix has the form,

$$A=\begin{pmatrix}1&0&0&c\\0&1&0&-b\\0&0&1&a\end{pmatrix},$$

where a,b and c are positive constants. The τ-function is then given by

$$\tau=E(1,2,3)+aE(1,2,4)+bE(1,3,4)+cE(2,3,4),$$

with $E(l,m,n)=(k_n-k_m)(k_n-k_l)(k_m-k_l)E_lE_mE_n$. This gives $(1,3)$-soliton solution which is dual to the case of $N=1$, that is, $[1,4]$-soliton for $y\ll 0$ and $[1,2]$-, $[2,3]$- and $[3,4]$-solitons for $y\gg 0$. The corresponding label for this solution is given by $\pi=(2\,3\,4\,1)$. The lower figures in Figure 3.2 shows the time-evolution of this type. Here we set a,b,c of the A-matrix as

$$a=\frac{|1,2,3|}{|1,2,4|},\quad b=\frac{|1,2,3|}{|1,3,4|},\quad c=\frac{|1,2,3|}{|2,3,4|},$$

where $|l,m,n|:=|(k_n-k_m)(k_n-k_l)(k_m-k_l)|$, so that all four solitons meet at the origin at $t=0$.

3.3. $N=2$ and $M=4$ cases

By a direct construction of the derangements of S_4 with two exedances (i.e. $N=2$), one can easily see that there are seven cases with 2×4 irreducible and totally non-negative A-matrices. Then the classification theorems imply that we have a $(2,2)$-soliton solution associated to each of those A-matrices. We here discuss all of those $(2,2)$-soliton solutions with the same k-parameters given by $(k_1,k_2,k_3,k_4)=(-\frac{7}{4},-\frac{1}{4},\frac{3}{4},\frac{3}{2})$, and show how each A-matrix chooses a particular set of line-solitons. In Figure 3.3, we illustrate the corresponding chord diagrams for all those seven cases, from which one can find the asymptotic line-solitons in each case.

3.3.1. The case $\pi=(3412)$

From the chord diagram in Figure 3.3, one can see that the asymptotic line-solitons are given by $[1,3]$- and $[2,4]$-types for both $y\to\pm\infty$. The solution in this case corresponds to the top cell of $\mathrm{Gr}(2,4)$, and the A-matrix is given

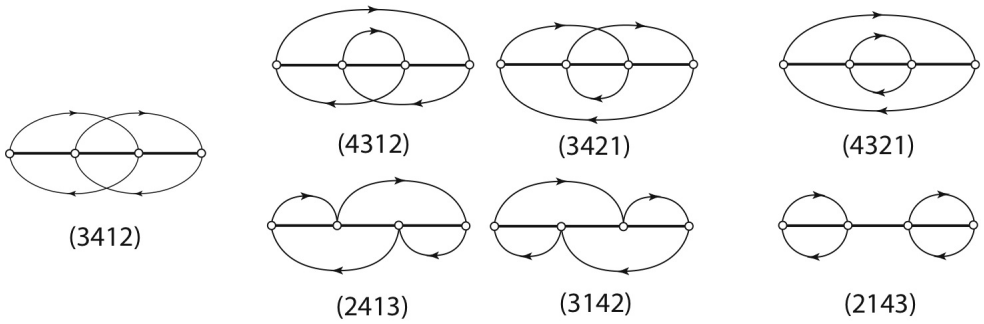

Figure 3.3: The chord diagrams for seven different types of $(2,2)$-soliton solutions. Each diagram parametrizes a unique cell in the totally non-negative Grassmannian $\mathrm{Gr}(2,4)$.

by

$$A = \begin{pmatrix} 1 & 0 & -c & -d \\ 0 & 1 & a & b \end{pmatrix},$$

where $a, b, c, d > 0$ are free parameters with $D := ad - bc > 0$. This is the generic solution on the maximal dimensional cell, and it is called T-type (after [9]). The most important feature of this solution is the generation of four intermediate solitons forming a box at the intersection point. Those intermediate solitons are identified as $[1,2]$-, $[2,3]$-, $[1,4]$- and $[3,4]$-solitons, and they may be obtained by *cutting* the chord diagram of (3412)-type at the crossing points. For example, if we cut the chords of $[1,3]$ and $[2,4]$ at the crossing point, we obtain either pair of $\{[1,2],[3,4]\}$ or $\{[1,4],[2,3]\}$. The first pair appears in the lower and upper edge of the box, and the second pair in the right and left edges. Figure 3.4 shows the time-evolution of the solution of this type. The parameters a, b, c and d in the A-matrix determine the locations of solitons, their phase shifts and the on-set of the box-shaped interaction pattern: Those are given by

$$b = \frac{|2,1|}{|4,1|} s e^{\Theta^+_{[1,3]}}, \quad c = \frac{|2,1|}{|3,2|} s e^{\Theta^+_{[2,4]}}, \quad \frac{a}{d} = \frac{|4,2|}{|3,1|} r, \quad D = \frac{|2,1|}{|4,3|} s, \tag{3.3}$$

where s is for the phase shift, $\Theta^+_{[i,j]}$ for the location of $[i,j]$-soliton for $x \gg 0$ (recall the definition below (2.10), i.e. $x^+_{[i,j]} = -\frac{1}{|j,i|}\Theta^+_{[i,j]}$ gives the x-intercept of the line of the $[i,j]$-soliton for $x \gg 0$ at $t = 0$), and r for the on-set of the box. The phase shifts for $[1,3]$- and $[2,4]$-solitons are given by $\Delta x_{[i,j]} := x^-_{[i,j]} - x^+_{[i,j]} = -\frac{1}{|j,i|}\Theta_{\mathrm{T}}$ with

$$\Theta_{\mathrm{T}} = \ln\left(\frac{|1,4||2,3|}{|1,2||3,4|}\,\frac{bc}{D}\right). \tag{3.4}$$

In Figure 3.4, we have chosen those parameters as $s = 1, \Theta^+_{[1,3]} = \Theta^+_{[2,4]} = 0$ and $r = 1$, so that at $t = 0$ the solution forms an X-shape without phase shifts and opening of a box at the origin. In Figure 3.4, the amplitudes are $A_{[1,3]} = \frac{25}{8}$ and $A_{[2,4]} = \frac{49}{36}$. Among the soliton solutions for $N = 2$ and $M = 4$, this solution is the most complicated and

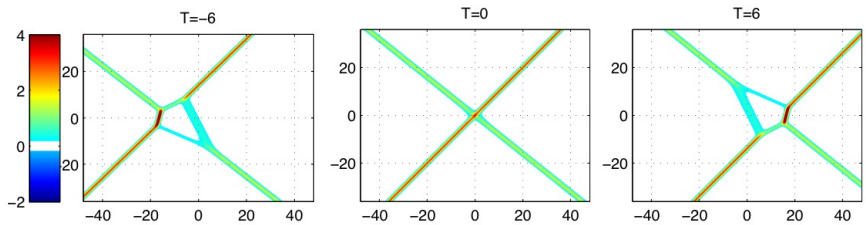

Figure 3.4: Example of (3412)-type soliton solution (T-type). The asymptotic solitons are $[1,3]$- and $[2,4]$-types for both $y \to \pm\infty$. The intermediate solitons forming a box-shape pattern are given by $[1,2]$-,$[1,4]$-, $[2,3]$- and $[3,4]$-solitons.

interesting one. As you can see below, this solution contains all other solutions as some parts of this solution, that is, as explained above, all six possible solitons (i.e. $\binom{4}{2} = 6$) appear in this solution.

3.3.2. The case $\pi = (4312)$

From the chord diagram in Figure 3.3, one can see that the asymptotic line-solitons are given by $[1,4]$- and $[2,3]$-solitons for $y \gg 0$ and $[1,3]$- and $[2,4]$-solitons in $y \ll 0$. The A-matrix in this case is given by

$$A = \begin{pmatrix} 1 & 0 & -b & -c \\ 0 & 1 & a & 0 \end{pmatrix},$$

where $a, b, c > 0$ are free parameters. Figure 3.5 illustrates an example of this solution. The parameters in the A-matrix

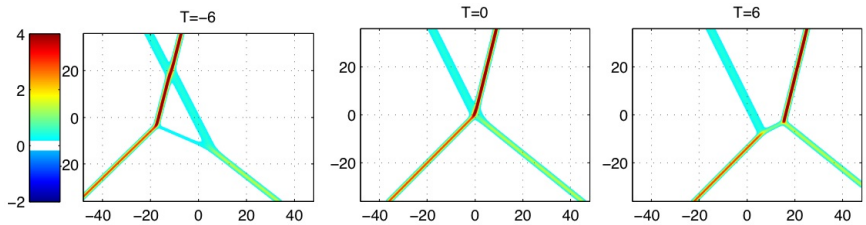

Figure 3.5: Example of (4312)-type soliton solution. The asymptotic solitons are $[1,4]$- and $[2,3]$-types for $y \gg 0$ and $[1,3]$- and $[2,4]$-types for $y \ll 0$. The intermediate solitons are $[3,4]$-type for $t = -6$ and $[1,2]$-type for $t = 6$.

determine the locations of the line-solitons in the following form,

$$a = \frac{|2,1|}{|3,1|} e^{\Theta^-_{[2,3]}}, \quad b = \frac{|2,1|}{|3,2|} e^{\Theta^-_{[1,3]}} \quad \text{and} \quad c = \frac{|3,1|}{|4,3|} e^{\Theta^+_{[1,4]}}.$$

The $\Theta^\pm_{[ij]}$ represent the locations of the $[i,j]$-soliton for $x \gg 0$ and $x \ll 0$, and the three line-solitons determine the location of the other one. We here take the parameters $\Theta^-_{[1,3]} = \Theta^+_{[1,4]} = \Theta^-_{[2,3]} = 0$, so that all those four solitons meet at the origin at $t = 0$. Notice here that the pattern in the lower part ($y < 0$) of the solution is the same as that of the previous one, T-type. This can be also seen by comparing the chord diagrams of those two cases.

3.3.3. The case $\pi = (3421)$

The asymptotic line-solitons in this case are given by $[1,3]$- and $[2,4]$-solitons for $y \gg 0$ and $[1,4]$- and $[2,3]$-solitons in $y \ll 0$. The A-matrix has the form,

$$A = \begin{pmatrix} 1 & 0 & 0 & -c \\ 0 & 1 & a & b \end{pmatrix},$$

where $a, b, c > 0$ are free parameters. Figure 3.6 illustrates the evolution of the solution of this type. The parameters

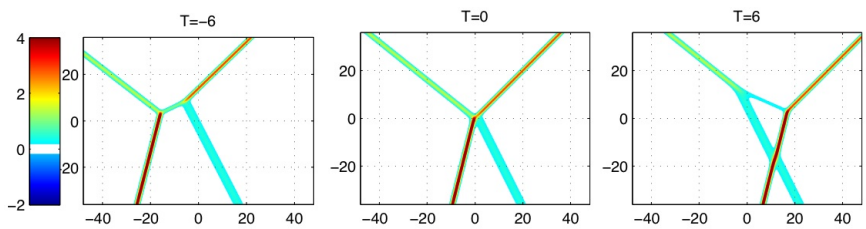

Figure 3.6: Example of (3421)-type soliton solution. The asymptotic solitons are given by $[1,3]$-and $[2,4]$-types for $y \gg 0$ and $[1,4]$- and $[2,3]$-types for $y \ll 0$. This solution is *dual* to the previous one of (4312)-type, i.e. the duality is given by $(x, y, t) \to (-x, -y, -t)$.

in the A-matrix are related to the locations of the line-solitons,

$$a = \frac{|2,1|}{|3,1|} e^{\Theta^+_{[2,3]}}, \quad b = \frac{|2,1|}{|4,1|} e^{\Theta^-_{[2,4]}} \quad \text{and} \quad c = \frac{|2,1|}{|4,2|} e^{\Theta^-_{[1,4]}}.$$

This solution can be considered as a dual of the previous case (b), that is, two sets of line-solitons for $y \gg 0$ and $y \ll 0$ are exchanged. Here we take $\Theta^{\pm}_{[i,j]} = 0$ for those pairs $(i, j) = (1, 4), (2, 3)$ and $(2, 4)$, hence all those four solitons meet at the origin at $t = 0$. Note here that now the upper pattern of the solution is the same as that of the T-type. So if one cuts Figures 3.5 and 3.6 along the x-axis and glues the lower half of Figure 3.5 together with the upper half of Figure 3.6, we can obtain Figure 3.4 (T-type). This can be observed from the corresponding chord diagrams.

One should also note that this solution is "dual" to the previous one in the sense that the patterns of those solutions are symmetric with respect to the change $(x, y, t) \leftrightarrow (-x, -y, -t)$.

3.3.4. The case $\pi = (2413)$

The asymptotic line-solitons are given by $[1, 2]$- and $[2, 4]$-solitons for $y \gg 0$ and $[1, 3]$- and $[3, 4]$-solitons for $y \ll 0$. The A-matrix is given by

$$A = \begin{pmatrix} 1 & 0 & -c & -d \\ 0 & 1 & a & b \end{pmatrix},$$

where $a, b, c, d > 0$ with $ad - bc = 0$. Those parameters are related to the locations of the line-solitons,

$$b = \frac{|2, 1|}{|4, 1|} e^{\Theta^-_{[2,4]}}, \quad c = \frac{|2, 1|}{|3, 2|} e^{\Theta^-_{[1,3]}} \quad \text{and} \quad \frac{d}{b} = \frac{|4, 1|}{|4, 2|} e^{\Theta^+_{[1,2]}},$$

with $a = bc/d$. Figure 3.7 illustrates the evolution of the solution of this type. For the case that all the solitons meet at

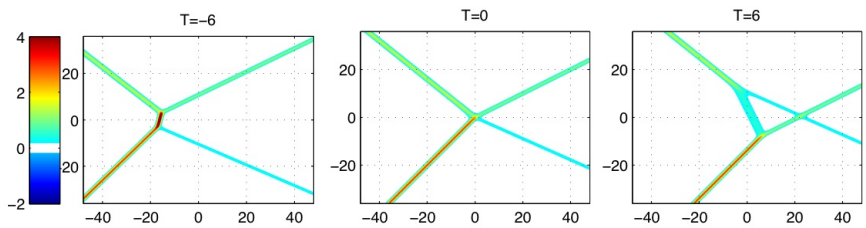

Figure 3.7: Example of (2413)-type soliton solution. The asymptotic solitons are $[1, 2]$- and $[2, 4]$-types for $y \gg 0$ and $[1, 3]$- and $[3, 4]$-types for $y \ll 0$. The intermediate solitons are $[1, 4]$-type in $t = -6$ and $[2, 3]$-type in $t = 6$.

the origin at $t = 0$, we set all $\Theta_{[i,j]}$ to be zero. Notice that the nonlinear interaction generates the intermediate soliton of $[1, 4]$-type in $t < 0$. This has the maximum amplitude among the (local) solitons appearing in the solution. It is interesting to note that the maximum amplitude soliton might be expected from the chord diagram, that is, this soliton is generated by the resonant interactions of $[1, 2] + [2, 4] = [1, 4]$ for $y > 0$ and $[1, 3] + [3, 4] = [1, 4]$ for $y < 0$. One should also note that the left patterns in Figure 3.7 including $[1, 4]$-soliton for $t < 0$ and $[2, 3]$-soliton for $t > 0$ are the same as those in Figure 3.4 (T-type).

3.3.5. The case $\pi = (3142)$

The asymptotic line-solitons are given by $[1, 3]$- and $[3, 4]$-solitons in $y \gg 0$ and $[1, 2]$- and $[2, 4]$-solitons in $y \ll 0$. The A-matrix has the form,

$$A = \begin{pmatrix} 1 & a & 0 & -c \\ 0 & 0 & 1 & b \end{pmatrix},$$

where $a, b, c > 0$. We represent those parameters in the following form which is particularly useful for our stability problem discussed in the next section,

$$a = \frac{|3, 1|}{|3, 2|} s e^{\Theta^+_{[2,4]}}, \quad b = \frac{|3, 1|}{|4, 1|} s e^{\Theta^+_{[1,3]}} \quad \text{and} \quad c = \frac{|3, 1|}{|4, 3|} s. \tag{3.5}$$

Here $\Theta^+_{[i,j]}$ represent the location of the $[i, j]$-soliton in $x \gg 0$, and s represents the location of the other line-solitons in $x \ll 0$, that is the generation of the intermediate line-solitons either $[1, 4]$- or $[2, 3]$-type (c.f. the case (c) in Section 5). This solution is dual to the previous one of $\pi = (2413)$. In fact, Figure 3.8 illustrates the dual behavior of the evolution in the sense of the reverse of time. Here we take $s = 1$ and $\Theta^+_{[1,3]} = \Theta^+_{[2,4]} = 0$, so that all solitons meet

at the origin at $t = 0$. As in the previous case, the large amplitude soliton of $[1, 4]$-type is generated by the resonant interaction. In particular, this solution can be used to explain the Mach reflection observed in shallow water [11, 5, 3].

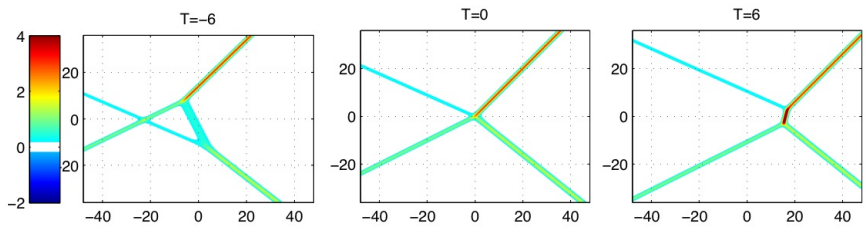

Figure 3.8: Example of (3142)-type soliton solution. The asymptotic solutions are $[1, 3]$- and $[3, 4]$-types for $y \gg 0$ and $[1, 2]$- and $[2, 4]$-types for $y \ll 0$. Notice the duality of this with (2413)-type in the previous example.

3.3.6. The case $\pi = (4321)$

The asymptotic line-solitons are $[1, 4]$- and $[2, 3]$-types for both $y \to \pm\infty$. Since those solitons can be placed both in nearly parallel to the y-axis, this type of solutions fits better in the *physical* assumption for the derivation of the KP equation, i.e. a quasi-two dimensionality. This is then referred to as P-type (after [9]). The situation is similar to the KdV case, for example, two solitons must have different amplitudes, $A_{[1,4]} > A_{[2,3]}$. The A-matrix is given by

$$A = \begin{pmatrix} 1 & 0 & 0 & -b \\ 0 & 1 & a & 0 \end{pmatrix}.$$

The parameters are expressed by

$$a = \frac{|4, 2|}{|4, 3|} e^{\Theta^+_{[2,3]}} \quad \text{and} \quad b = \frac{|3, 1|}{|4, 3|} e^{\Theta^+_{[1,4]}}. \tag{3.6}$$

where $\Theta^+_{[i,j]}$ represents the location of the $[i, j]$-soliton in $x > 0$ (the wave front) (notice the phase shifts for the solitons). Figure 3.9 illustrates the evolution of the solution of this type. We here set $\Theta^+_{[i,j]} = 0$, and hence the solitons

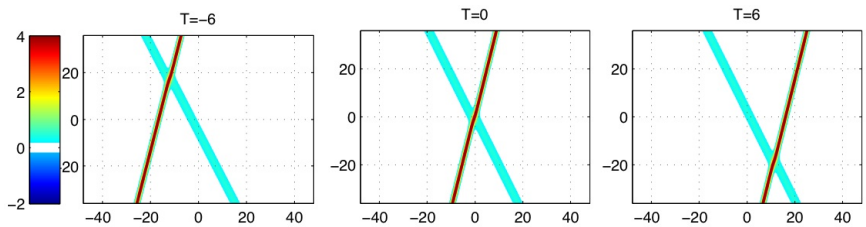

Figure 3.9: Example of (4321)-type soliton solution (P-type). The asymptotic solitons are $[1, 4]$- and $[2, 3]$-types for both $y \to \pm\infty$. The pattern of the solution is stationary, and the interaction generates a negative phase shift of the solitons.

in $x > 0$ (the wave front) meet at the origin at $t = 0$. Note here that there is a phase shift due to the interaction, and the shift is in the negative direction due to the repulsive force in the interaction similar to the case of KdV solitons. The phase shifts are given by $\Delta x_{[i,j]} = -\frac{1}{|j,i|}\Theta_{\mathrm{P}}$ with

$$\Theta_{\mathrm{P}} = \ln\left(\frac{|4, 2||3, 1|}{|2, 1||4, 3|}\right) > 0. \tag{3.7}$$

This negative phase shift is due to the *repulsive* force in the interaction as in the case of the KdV solitons. One should also note that the interaction point moves in the negative y-direction, because the larger soliton of $[1, 4]$-type propagates faster than the other one. Those $[1, 4]$- and $[2, 3]$-solitons only appear as the intermediate solitons in the solution of T-type, that is, they form a part of the box in Figure 3.4.

3.3.7. The case $\pi = (2143)$

The asymptotic line-solitons are $[1,2]$- and $[3,4]$-types for both $y \to \pm\infty$. This solution was used *originally* to describe two soliton solution, and it is called O-type (after [9]). Interaction properties for solitons with equal amplitude has been discussed using this solution. However this solution becomes singular, when those solitons are almost parallel to each other and close to the y-axis, contrary to the assumption of the quasi-two dimensionality for the KP equation [11]. The A-matrix is given by

$$A = \begin{pmatrix} 1 & a & 0 & 0 \\ 0 & 0 & 1 & b \end{pmatrix}.$$

Notice that this A-matrix is the limit of that for (3142)-type with $c \to 0$ and $k_2 \to k_3$. We will further discuss this issue in the next section when we study the initial value problem with V-shape initial wave. The parameters a and b are expressed by

$$a = \frac{|4,1|}{|4,2|} e^{\Theta^+_{[1,2]}} \quad \text{and} \quad b = \frac{|3,2|}{|4,2|} e^{\Theta^+_{[3,4]}}. \tag{3.8}$$

where $\Theta^+[i,j]$ represents the location of the wave front consisting of $[1,2]$- and $[3,4]$-solitons. Figure 3.10 illustrates the evolution of this type solution. Here we take all $\Theta^+_{[i,j]} = 0$, the solitons in $x > 0$ (the wave front) meet at the origin

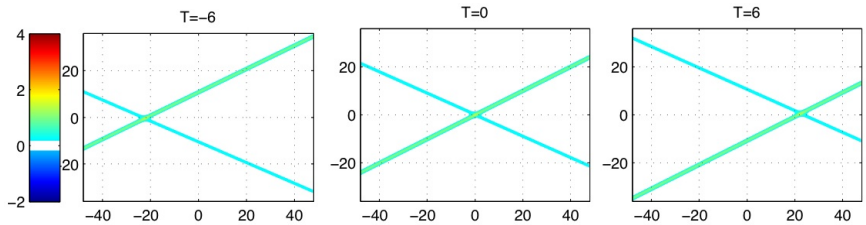

Figure 3.10: Example of (2143)-type soliton solution (O-type). The asymptotic solitons are $[1,2]$- and $[3,4]$-types for both $y \to \pm\infty$. The pattern of the solution is stationary, and has a positive phase shift in the solitons.

at $t = 0$. The phase shifts of those solitons are positive due to an *attractive* force in the interaction, and they are given by $\Delta x_{[i,j]} = -\frac{1}{|j,i|}\Theta_{\mathrm{O}}$ with

$$\Theta_{\mathrm{O}} = \ln\left(\frac{|4,1||3,2|}{|3,1||4,2|}\right) < 0. \tag{3.9}$$

When k_2 approaches to k_3, the phase shift gets larger, and the interaction part of the solution is getting to be close to $[1,4]$-soliton as a result of the resonant interaction with $[1,2]$- and $[3,4]$-solitons at $k_2 = k_3$. This is the main argument of the paper [11] about the discussion on the Mach reflection of shallow water waves. Note also that those $[1,2]$- and $[3,4]$-solitons appear as the intermediate solitons forming a box of T-type as shown in Figure 3.4.

4. Numerical simulations

The main purpose of the numerical simulation is to study the interaction properties of line-solitons, and we will show that the solution of the initial value problem with certain types of initial waves asymptotically approaches to some of the exact solutions discussed in the previous section. This implies a stability of those exact solutions under the influence of certain deformations (notice that the deformations in our initial waves are not so small).

The initial value problem considered here is essentially an infinite energy problem in the sense that each line-soliton in the initial wave is supported asymptotically in either $y \gg 0$ or $y \ll 0$, and the interactions occur only in a finite domain in the xy-plane. In the numerical scheme, we consider the rectangular domain $D = \{(x,y) : |x| \le L_x,\ |y| \le L_y\}$, and each line-soliton is matched with a KdV soliton at the boundaries $y = \pm L_y$. In this section, we explain the details of our numerical scheme and give an error estimate of the scheme.

4.1. Numerical scheme

Using the so-called *window technique* [17, 19], we first transform our non-periodic solution u having non-vanishing boundary values into a function v rapidly decaying near the boundaries $y = \pm L_y$, so that we consider the function v to be periodic in both x and y. With the window function $W(y)$, this can be expressed by the decomposition of the solution u, i.e.

$$u = v + (1 - W)u \quad \text{with} \quad v = Wu.$$

We take the window function $W(y)$ in the form of a super-Gaussian,

$$W(y) = \exp\left(-a_n \left|\frac{y}{L_y}\right|^n\right), \tag{4.1}$$

where a_n and n are positive constants (we choose $a_n = (1.111)^n \ln 10$ with $n = 27$ [19]).

We assume that near the boundaries $y = \pm L_y$, the solution can be described by exact line-solitons (i.e. we take L_y large enough so that the interaction will not influence those parts near boundaries up to certain finite time). We then consider the transformation in the form,

$$u = v + (1 - W)u_0, \tag{4.2}$$

where u_0 consists of exact line-solitons satisfying

$$(1 - W)u_0 = (1 - W)u.$$

This assumption prevents any disturbance from the boundary, and keeps the stability of the far fields consisting of well separated line-solitons. We are interested in studying an asymptotic behavior near the interaction point, and we do not expect to see any strong effect from the boundary region in a short time (recall that the system has a finite group velocity for waves with non-zero k_x-component).

With the transformation (4.2), we have the equation for v,

$$\begin{aligned} &\partial_x \left(4\partial_t v + 6v\partial_x v + \partial_x^3 v\right) + 3\partial_y^2 v \\ &= 6(1 - W)\partial_x \left(Wu_0\partial_x u_0 - \partial_x(vu_0)\right) + 3(2W'\partial_y u_0 + W'' u_0). \end{aligned} \tag{4.3}$$

Assuming the solution v to be periodic in both x and y with zero boundary condition at $|y| = L_y$, we solve (4.3) by using fast Fourier transform (FFT). For a convenience, let us rescale the domain $D = \{(x, y) : |x| \le L_x, |y| \le L_y\}$ with $\mathcal{D} := \{(X, Y) : |X| \le \pi,\ |Y| \le \pi\}$, i.e.

$$X = \frac{\pi}{L_x}x, \quad Y = \frac{\pi}{L_y}y.$$

Then (4.3) becomes

$$\partial_X \left(\partial_t v + Pv\partial_X v + Q\partial_X^3 v\right) + R\partial_Y^2 v = F, \tag{4.4}$$

where F is the right hand side of (4.3) with the scalings, and

$$P = \frac{3\pi}{2L_x}, \quad Q = \frac{\pi^3}{4L_x^3}, \quad \text{and} \quad R = \frac{3\pi L_x}{4L_y^2}.$$

Under the periodic assumption of v, we have

$$v(X, Y, t) = \sum_{l=-\infty}^{\infty} \sum_{m=-\infty}^{\infty} \hat{v}(l, m, t)e^{i(lX+mY)}.$$

Here the Fourier transformation $\hat{v} := \mathcal{F}(v)$ is given by

$$\hat{v}(l, m, t) = \frac{1}{(2\pi)^2} \int_{-\pi}^{\pi} \int_{-\pi}^{\pi} v(X, Y, t)e^{-i(lX+mY)} dX dY,$$

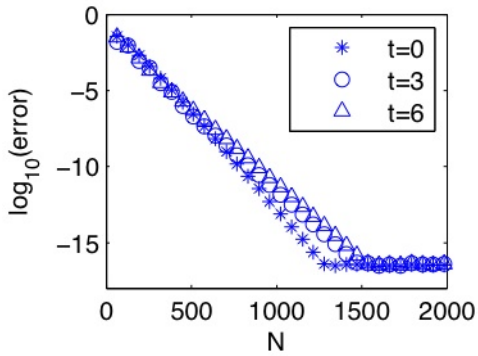

Figure 4.1: Numerical accuracy test on T-type solution shown in Fig. 3.4. The graph shows the estimate of $\max|\mathcal{F}(v^t) - \mathcal{F}(v^t_{\text{exact}})|$ as a function of the number of Fourie modes $N \times N/2$ for $t = 0, 3$ and 6. The error is decreasing exponentially with respect to N until it saturates at round of error $\approx 10^{-16}$ for $N \approx 1280, 1472$ and 1536 for $t = 0, 3$ and 6, respectively. The numerical domain is $D = [-64, 64] \times [-32, 32]$.

and the equation becomes

$$\partial_t \hat{v} + i\left(\frac{Rm^2}{2l} - Ql^3\right)\hat{v} + il\frac{P}{2}\mathcal{N}(\hat{v}) = \frac{1}{il}\mathcal{F}(F),$$

with

$$\mathcal{N}(\hat{v}) = \mathcal{F}(v^2).$$

Let $c = \frac{Rm^2}{2l} - Ql^3$ and $\hat{V} = e^{ict}\hat{v}$. Then we have

$$\partial_t \hat{V} + il\frac{P}{2}e^{ict}\mathcal{N}(\hat{v}) = \frac{1}{il}e^{ict}\mathcal{F}(F). \tag{4.5}$$

We write this equation in the form of time evolution,

$$\partial_t \hat{V} = G(t, \hat{V}).$$

and use the 4-th order Runge-Kutta (RK4) method to solve the equation: Namely denoting $t_n = n\Delta t$ and

$$K_1 = G\left(t_n, \hat{V}_n\right), \quad K_2 = G\left(t_n + \frac{1}{2}\Delta t, \hat{V}_n + \frac{K_1}{2}\Delta t\right),$$
$$K_3 = G\left(t_n + \frac{1}{2}\Delta t, \hat{V}_n + \frac{K_2}{2}\Delta t\right), \quad K_4 = G\left(t_n + \Delta t, \hat{V}_n + \frac{K_3}{2}\Delta t\right),$$

we have

$$\hat{V}_{n+1} = \hat{V}_n + \frac{1}{6}\left[K_1 + 2(K_2 + K_3) + K_4\right]\Delta t.$$

We use a pseudo-spectral method to evaluate nonlinear term $\mathcal{N}(\hat{v})$ in (4.5) and the 2nd order central difference to approximate three derivative terms in the F on the right hand side of (4.4) for simplicity. This is because u_0 in (4.2) is a non-periodic function and the estimation of derivatives from a Fourier spectral method still introduces errors at the computational boundary. A better choice is to provide the exact closed forms for the x-and y-derivatives of u_0. Since some of the exact solutions have rather complicated formulae, we simply use 2nd order central difference approximation. Thus the numerical solutions are expected to be of 2nd order accuracy when there are enough Fourier modes in space and the solutions are vanished in large x.

In order to verify the accuracy of the method, we provide two tests. The first test intends to answer the question on how many Fourier modes are needed to ensure machine accuracy in space for the solution v of (4.3). The second test shows the overall algorithm is 2nd order accurate. In Figure 4.1, we show the maximum error in the Fourier modes of the T-type solution in the sense that we estimate $\max|\mathcal{F}(v) - \mathcal{F}(v_{\text{exact}})|$ with respect to the number of Fourier modes N in both x- and y-directions for the case shown in Figure 3.4. On the computational domain $D = [-64, 64] \times [-32, 32]$,

	$\Delta t = 10^{-2}$	$\Delta t = 5 \times 10^{-3}$	order
$t = 1$	1.046×10^{-2}	2.645×10^{-3}	1.98
$t = 2$	1.893×10^{-2}	4.353×10^{-3}	2.12
$t = 3$	2.507×10^{-2}	5.986×10^{-3}	2.07
$t = 4$	2.992×10^{-2}	7.732×10^{-3}	1.95
$t = 5$	3.523×10^{-2}	9.675×10^{-3}	1.86
$t = 6$	4.211×10^{-2}	1.194×10^{-2}	1.82

Table 1: The convergence test on the domain $D = [-128, 128] \times [-16, 16]$ with 2048×256 Fourier modes. The graph shows the error $\|u^t - u^t_{\text{exact}}\|_{L^2(D)}/\|u^t_{\text{exact}}\|_{L^2(D)}$ for the time steps $\Delta t = 0.01$ and 5×10^{-3}. This indicates that our scheme is of 2nd order accurate in time.

machine accuracy $\approx 10^{-16}$ is reached for $N \approx 1280, 1472$ and 1536 for $t = 0, 3$ and 6, respectively. Since the T-type solution develops a box at later time, it requires more Fourier modes to well represent the solution. From this test with $N = 1536$, we find that we need roughly $\frac{1536}{2\times 64} = 12$ Fourier modes per 1 unit in x to reach 10^{-16} accuracy. Notice that it might take longer time to run such a fine mesh for a very large computational domain. If we choose to use 8 Fourier modes per unit length in both x- and y-directions, the spacial error is within 10^{-10} and it can also speed up the computation. In Table 1, we summarize the error of the solution given by $\|u^t - u^t_{\text{exact}}\|_{L^2(D)}/\|u^t_{\text{exact}}\|_{L^2(D)}$ for two different time steps $\Delta t = 0.01$ and $\Delta t = 5 \times 10^{-3}$ on $D = [-128, 128] \times [-16, 16]$ with 2048×256 Fourier modes. It can be clearly seen that the order of convergence is 2 because the error decreases by a factor around 4 when the time step is halved. If we take $\Delta t = 5 \times 10^{-3}$ and keep running the simulation up to $t = 12$, the magnitude of the error is always within 2.5×10^{-2}. In the following simulations, the errors of the solutions are at this magnitude or smaller.

5. Numerical results

Now we present the results of the direct numerical simulation of the KP equation with the following two types of initial waves consisting of two line-solitons. In particular, we fix the amplitude of one of the line-solitons, and place these line-solitons in the symmetric shape with respect to the x-axis. This then implies that each profile of the initial wave is determined by two parameters A_0 (the amplitude of other soliton) and Ψ_0 (the angle of the wave-vector of the soliton):

(i) V-shape wave consisting of two semi-infinite line-solitons, i.e. $u(x, y, 0) = u^0_1(x, y) + u^0_2(x, y)$ with

$$\begin{cases} u^0_1(x, y) = A_0 \operatorname{sech}^2 \sqrt{\dfrac{A_0}{2}}(x - y \tan \Psi_0) \times H(y), \\ u^0_2(x, y) = 2 \operatorname{sech}^2(x + y \tan \Psi_0) \times H(-y), \end{cases} \tag{5.1}$$

where $H(z)$ is the unit step function,

$$H(z) = \begin{cases} 1 & \text{if} \quad z \geq 0, \\ 0 & \text{if} \quad z < 0. \end{cases}$$

Here one should note that the initial locations $x^+_{[i,j]}$ are zero for both line-solitons, that is, they cross the origin at $t = 0$. The shifts of $x^+_{[i,j]}$ observed in the simulations provide the information of the interaction property.

(ii) X-shape wave of the linear combination of two line-solitons, i.e. $u(x, y, 0) = u^0_1(x, y) + u^0_2(x, y)$ with

$$\begin{cases} u^0_1(x, y) = A_0 \operatorname{sech}^2 \sqrt{\dfrac{A_0}{2}}(x - y \tan \Psi_0), \\ u^0_2(x, y) = 2 \operatorname{sech}^2(x + y \tan \Psi_0). \end{cases} \tag{5.2}$$

Again note that the initial locations are $x^+_{[i,j]} = 0$.

These initial waves have been considered in certain physical models of interacting waves [11, 5, 16, 18, 3]. In particular, in [16, 18], the V-shape initial waves were considered to study the generation of large amplitude waves in shallow water.

The main result of this section is to show numerically that those initial waves *converge* asymptotically to some of the exact solutions presented in Section 3. Here what we mean by the *convergence* is as follows: We first show that the solution $u^t(x, y)$ at the intersection point of V- or X-shape generates a pattern due to the resonant interaction, and we then identify the pattern near the resonant point with that given by some of the exact solutions $u^t_{\text{exact}}(x, y)$. The convergence is only in a local sense, and we use the following (relative) error estimate,

$$E(t) := \|u^t - u^t_{\text{exact}}\|^2_{L^2(D^t_r)} / \|u^t_{\text{exact}}\|^2_{L^2(D^t_r)}, \tag{5.3}$$

where D^t_r is the circular disc defined by

$$D^t_r := \left\{(x, y) \in \mathbb{R}^2 : (x - x_0(t))^2 + (y - y_0(t))^2 \le r^2\right\}.$$

Here the center $(x_0(t), y_0(t))$ is chosen as the intersection point of two lines determined from the corresponding exact solution identified by the following steps:

1. For a given initial wave, we first identify the type of exact solution (i.e. the chord diagram) from the formulae, $A_{[i,j]} = \frac{1}{2}(k_i - k_j)^2$ and $\tan \Psi_{[i,j]} = k_i + k_j$. This then gives the exact solution with the corresponding A-matrix. Note here that the entries of the A-matrix are not determined yet.

2. We then minimize the error function $E(t)$ of (5.3) at certain large time $t = T_0$ by changing the entries in the A-matrix, that is, we consider
$$\underset{A-\text{matrix}}{\text{Minimize}}\, E(T_0). \tag{5.4}$$
The minimization is achieved by adjusting the solution pattern with the exact one, that is, the pattern determines the A-matrix whose entries give the locations of all line-solitons including the intermediate solitons in the solution. With this A-matrix, the center $(x_0(t), y_0(t))$ of the circular domain D^t_r is given by the intersection point of the lines,
$$x + y \tan \Psi_{[i_l,j_l]} - C_{[i_l,j_l]} t = x^+_{[i_l,j_l]} \qquad \text{for} \quad l = 1, 2, \tag{5.5}$$
where the locations $x^+_{[i_l,j_l]}$ are expressed in terms of the A-matrix (see Section 3). Here we have $A_{[i_1,j_1]} = A_0$, $A_{[i_2,j_2]} = 2$ and $\Psi_{[i_2,j_2]} = -\Psi_{[i_1,j_1]} = \Psi_0$. The time T_0 may be taken as $T_0 = 0$, but for most of the cases, we need T_0 to be sufficiently large. This implies that the solutions have nontrivial location shifts, i.e. $x^+_{[i,j]} \neq 0$ in the solution.

3. We then confirm that $E(t)$ further decreases for a larger time $t > T_0$ up-to a time $t = T_1 > T_0$, just before the effects of the boundary enter the disc D^t_r (those effects include the periodic condition in x and a mismatch on the boundary patching).

We take the radius r in D^t_r large enough so that the main interaction area is covered for all $t < T_0$, but D^t_r should be kept away from the boundary to avoid any influence coming from the boundaries. The time $T_1 > T_0$ gives an enough time to develop a pattern close to the corresponding exact solution, but it is also limited to avoid any disturbance from the boundaries for $t < T_1$. In this paper, we give T_0 and T_1 based on the observation of the numerical results, and we will report the detailed analysis in a future communication.

5.1. V-shape initial waves

The initial wave form is illustrated in the left panel of Figure 5.1. The right figure shows the (incomplete) chord diagrams corresponding to the initial V-shape waves; that is, the upper chord represents the (semi-infinite) line-soliton in $y > 0$ and the lower one represents the (semi-infinite) line-soliton in $y < 0$. We have done the numerical simulations with six different cases which are marked in Figure 5.1 as (a) through (f). The main result in this section is to show that each *incomplete* chord diagram representing the initial wave gets a completion with minimum additional chords which represents the asymptotic pattern of the solution. Here the *minimal completion* implies that for a given incomplete chord diagram, one adds extra chords with minimum total length so that the complete chord diagram represents a derangement (see also [10]). For our examples of the cases (a) through (f), we have the following completions:

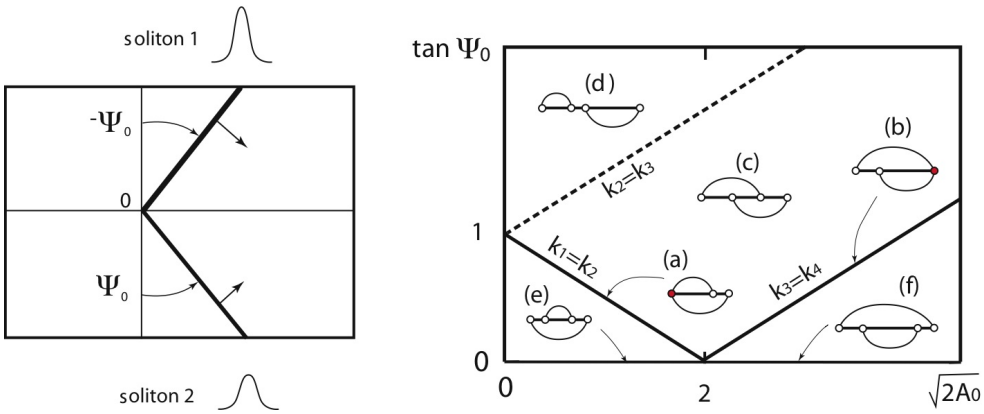

Figure 5.1: V-shape initial waves. Each line of the V-shape is a semi-infinite line-soliton. We set those line-solitons to meet at the origin, and fix the amplitude of the soliton in $y < 0$ to be 2. A_0 is the amplitude of the soliton in $y > 0$. The right panel shows the incomplete chord diagrams corresponding to the choice of the values A_0 and Ψ_0. There is no corresponding exact soliton solution on the dotted line of $k_2 = k_3$.

(a) With $k_1 = k_2$, the completion is $\pi = \begin{pmatrix} 1 & 3 & 4 \\ 3 & 4 & 1 \end{pmatrix}$, i.e. add $[3, 4]$-chord in $y > 0$. This implies that $[3, 4]$-soliton appears in the asymptotic solution in y>0, and the corresponding exact solution is a $(1, 2)$-soliton (cf. Figure 3.1).

(b) With $k_3 = k_4$, the completion is $\pi = \begin{pmatrix} 1 & 2 & 3 \\ 3 & 1 & 2 \end{pmatrix}$, i.e. add $[1, 2]$-chord in $y < 0$ which appears in the asymptotic solution, and the corresponding solution is a $(2, 1)$-soliton (cf. Figure 3.1).

(c) The completion is $\pi = (3142)$, i.e. add $[1, 2]$-chord in $y < 0$ and $[3, 4]$-chord in $y > 0$. These corresponding solitons appear behind those initial solitons (cf. Figure 3.8).

(d) The completion is $\pi = (2143)$, i.e. add $[1, 2]$-chord in $y < 0$ and $[3, 4]$-chord in $y > 0$. The soliton solution is of O-type, and the semi-infinite initial solitons extend to generate other half with the phase shift (cf. Figure 3.10).

(e) The *minimal* completion is $\pi = (2341)$, i.e. add $[1, 2]$- and $[3, 4]$-chords in $y > 0$. This is a $(1, 3)$-soliton. (Note that the initial wave is a front half of P-type soliton solution, but the minimal completion is *not* of P-type.) Since $[1, 2]$-soliton in $y > 0$ appears ahead of the wavefront consisting of $[2, 3]$-soliton in $y > 0$ and $[1, 4]$-soliton in $y < 0$, the generation of $[1, 2]$-soliton is impossible. The $[1, 2]$-soliton is a *virtual* one, but it gives an influence on bending the $[1, 4]$-soliton in $y > 0$ (see below for the details).

(f) The *minimal* completion is $\pi = (4123)$, i.e. add $[1, 2]$- and $[3, 4]$-chords in $y < 0$. The is a $(3, 1)$-type, but again we note that $[3, 4]$-soliton in $y < 0$ is a virtual one (i.e. it locates ahead of the wavefront similar to the previous case (e)). We also observe the bending of $[1, 4]$-soliton in $y > 0$ under the influence of this virtual soliton (see again below for the details).

5.1.1. The case (a)

This is a critical case with $k_1 = k_2$. The line-solitons of V-shape initial wave are $[1, 3]$-soliton in $y > 0$ and $[1, 4]$-soliton in $y < 0$. We take the following values for the amplitudes and angles of the those solitons,

$$\begin{cases} A_{[1,3]} = A_0 = \frac{1}{2}, & \tan\Psi_{[1,3]} = -\frac{1}{2} = -\tan\Psi_0, \\ A_{[1,4]} = 2, & \tan\Psi_{[1,4]} = \frac{1}{2} = \tan\Psi_0. \end{cases}$$

With the formulas for the amplitude $A_{[i,j]} = \frac{1}{2}(k_i - k_j)^2$ and the angle $\tan\Psi_{[i,k]} = k_i + k_j$, we have the k-parameters $(k_1 = k_2, k_3, k_4) = (-\frac{3}{4}, \frac{1}{4}, \frac{5}{4})$. The corresponding exact solution is of $(1, 2)$-type.

The top figures of Figure 5.2 illustrate the result of the direct numerical simulation. The simulation shows a generation of third wave at the point of the intersection of those initial solitons. This generation is due to the resonant interaction, and this may be identified as $[3, 4]$-soliton of the exact solution, that is, the resonance condition gives

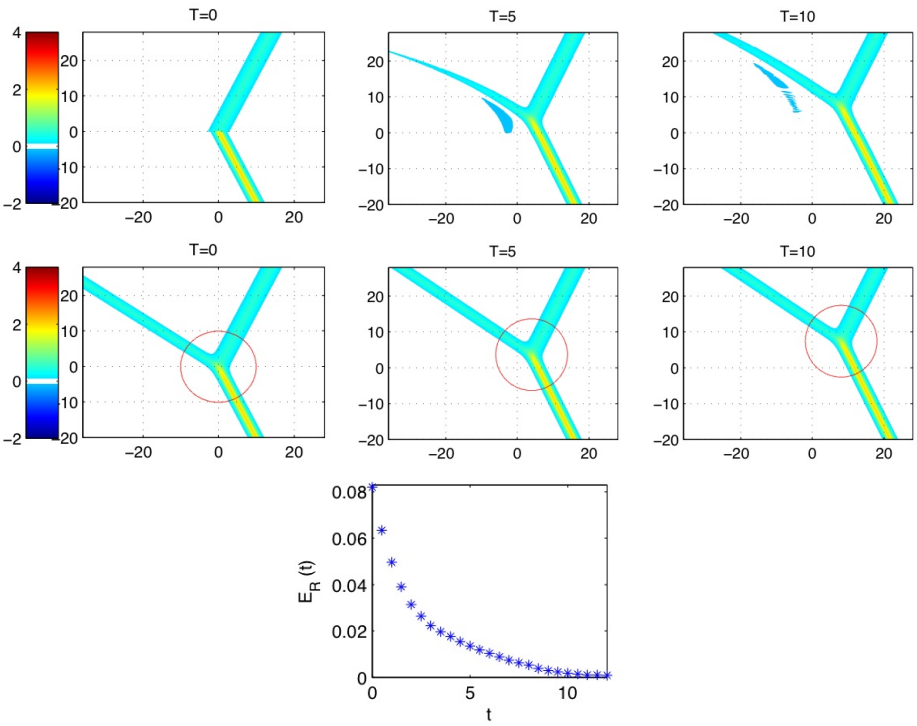

Figure 5.2: Numerical simulation of the case (a) in Figure 5.1: The initial wave consists of $[1,3]$-soliton in $y > 0$ and $[1,4]$-soliton in $y < 0$. The top figures show the result of the direct simulation, the middle figures show the corresponding exact solution of $(1,2)$-type, and the bottom one represents the error function $E(t)$ of (5.3) which is minimized at $t = 10$. The circles in the exact solution shows the domain D_r^t. A dispersive radiation appearing behind the interaction region may be considered as a reaction of the generation of the third soliton of $[3,4]$-type as a result of resonant interaction (see the text for the details).

$[1,3] + [3,4] = [1,4]$ and completes the incomplete chord diagram. The generation of $[3,4]$-soliton may be also understood by decomposing the exact solution into two parts, say $u_{\text{exact}} = u + v$, where u is the solution of the KP equation with our initial wave of $[1,3]$- and $[1,4]$-solitons. Then v satisfies,

$$\partial_x(4\partial_t v + 6v\partial_x v + \partial_x^3 v) + 3\partial_y^2 v = -6\partial_x^2(uv),$$

which is the KP equation with one extra term in the right hand side. If we assume that the initial solitons remain as the part of the exact solution u_{exact}, the product uv in the extra term has nonzero value only near the origin at $t = 0$ (this assumption is not totally correct, but the shifts of the initial solitons are very small for most of the cases). We then expect v to be close to the solution of the KP equation with the initial wave of $[3,4]$-soliton only for $y > 0$ and $x < 0$. Since this $[3,4]$-soliton is missing in the front half ($x > 0$), the edge of the wave gets a strong dispersive effect. Then the edge of the solution v disperses away with a bow-shape wake propagating toward the negative x-axis as can be seen in the simulation (cf. Figure 5.2). Recall here that the dispersive waves (i.e. non-soliton parts) propagate in the negative x-direction (see Section 3). Then the decay of the v solution at the front edge implies the appearance of the $[3,4]$-soliton in the exact solution as one can see from $u = u_{\text{exact}} - v$. This argument may be also applied to other cases as well.

Minimizing the error function $E(t)$ at $t = T_0 = 10$ with (5.4), we obtain the A-matrix of $(1,2)$-type,

$$A = \begin{pmatrix} 1 & 0 & -1.27 \\ 0 & 1 & 0.63 \end{pmatrix},$$

The minimization is achieved by adjusting the locations of the $[1,3]$- and $[1,4]$-solitons of the wavefront, and it gives the shifts

$$x_{[1,3]}^{+} = -0.0079, \qquad x_{[1,4]}^{+} = -0.120.$$

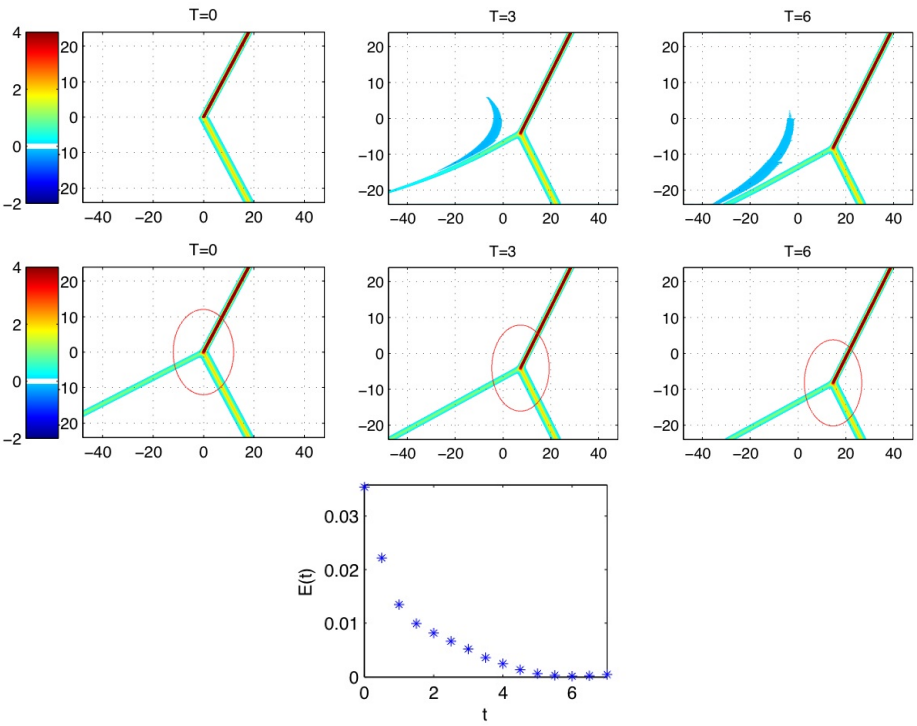

Figure 5.3: Numerical simulation of the case (b) in Figure 5.1: The initial wave consists of $[1,4]$- and $[2,4]$-solitons in $y > 0$ and $y < 0$ respectively. The top figures show the result of the direct simulation, and the middle figures show the corresponding exact solution of $(2,1)$-type. The bottom graph shows the error function $E(t)$ of (5.3) which is minimized at $t = 6$.

(The A-matrix is then obtained using (3.2)). Thus the new line-soliton of $[3,4]$-type has a relatively large negative shift. This may be explained as follows: The $[3,4]$-soliton is generated as a part of the tail of $[1,4]$-soliton, and in the beginning stage of the generation, the $[3,4]$-soliton has a small amplitude and propagates with slow speed. This causes a negative shift of this soliton. Also the negative shift in the $[1,4]$-soliton is due to the generation of the $[3,4]$-soliton, i.e. losing its momentum. The middle figures of Figure 5.2 show the exact solutions generated by the τ-function with those parameters $(k_1 = k_2, k_3, k_4) = (-\frac{3}{4}, \frac{1}{4}, \frac{5}{4})$ and the A-matrix given above. The circles in the figures show D_r^t where we take $r = 12$ and the center is given by $(x_0(t) = \frac{13}{16}t - 0.0637,\ y_0(t) = \frac{3}{4}t - 0.112)$. In the bottom figures of Figure 5.2, we plot the error function $E(t)$ of (5.3). Figure 5.2 indicates that the asymptotic solution seems to converge to the exact solution of $(1,2)$-type with the above A-matrix and the same k-parameters.

5.1.2. The case (b)

This is also a critical case with $k_3 = k_4$. The line-solitons of V-shape initial wave are $[1,3]$-soliton in $y > 0$ and $[2,3]$-soliton in $y < 0$. We take the amplitudes and angles of those solitons to be

$$\begin{cases} A_{[1,3]} = A_0 = \frac{49}{8}, & \tan\Psi_{[1,3]} = -\frac{3}{4} = -\tan\Psi_0, \\ A_{[2,3]} = 2, & \tan\Psi_{[2,3]} = \frac{3}{4} = \tan\Psi_0. \end{cases}$$

This then gives the k-parameters $(k_1, k_2, k_3 = k_4) = (-\frac{17}{8}, -\frac{5}{8}, \frac{11}{8})$. Figure 5.3 illustrates the result of the numerical simulation. The top figures show the direct simulation of the KP equation. Notice again that a bow-shape wake behind the interaction point corresponds to the v solution in the decomposition, $u = u_{\text{exact}} - v$, and the decay of v implies the appearance (or generation) of $[1,2]$-soliton. Notice that v gives the $[1,2]$-soliton part in the exact solution. The middle figures show the corresponding exact solution of $(2,1)$-type, whose A-matrix is obtained by minimizing the error function $E(t)$ at $t = 6$,

$$A = \begin{pmatrix} 1 & 1.15 & 1.21 \end{pmatrix}.$$

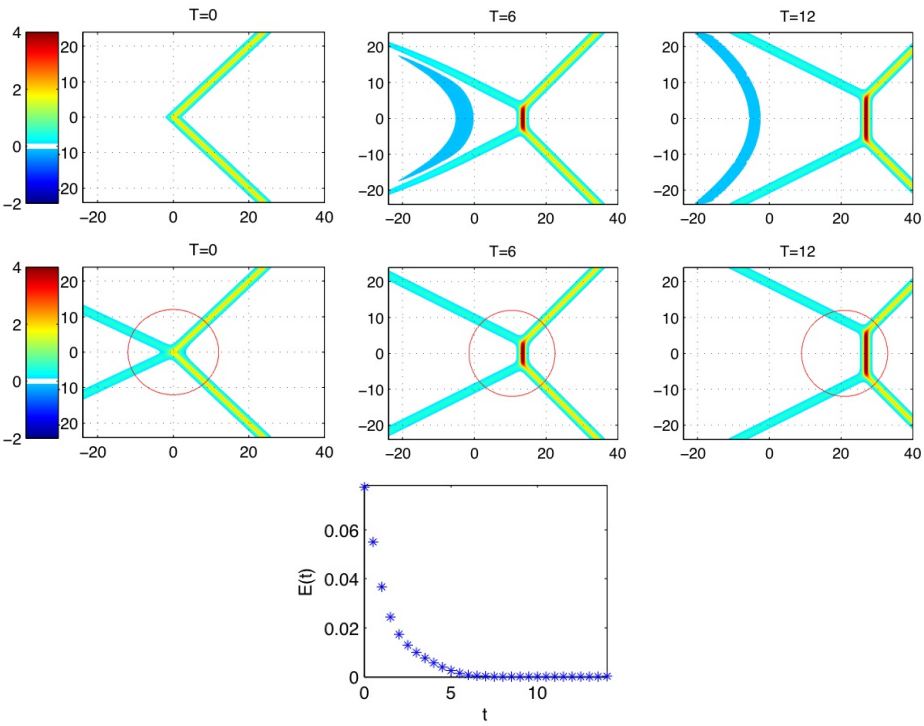

Figure 5.4: Numerical simulation of the case (c) in Figure 5.1: The initial wave consists of $[1,3]$-soliton in $y > 0$ and $[2,4]$-soliton in $y < 0$. The top figures show the result of the direct simulation, and the middle figures show the corresponding exact solution of (3142)-type. The bottom graph of the error function $E(t)$ which is minimized at $t = 10$. A large amplitude intermediate soliton is generated at the intersection point, and it corresponds to the $[1,4]$-soliton with the amplitude $A_{[1,4]} = 4.5$.

The shifts of locations $x^+_{[i,j]}$ obtained in the minimization are given by

$$x^+_{[1,3]} = -0.0545, \qquad x^+_{[2,3]} = -0.0254,$$

using (3.1). Those negative shifts may be explained in the similar way as in the previous case. In those figures, the domain D^t_r has $r = 12$ and its center $(x_0(t) = \frac{157}{64}t - 0.0399,\ y_0(t) = -\frac{11}{8}t + 0.0194)$. The bottom graph in Figure 5.3 shows that the solution converges asymptotically to the exact solution of $(2,1)$-type with the above A-matrix and the same k-parameters.

5.1.3. The case (c)

The line-solitons of the initial wave are $[1,3]$-soliton in $y > 0$ and $[2,4]$-soliton in $y < 0$. We consider the case with the larger soliton in $y > 0$, and take the amplitudes and angles of those solitons as

$$\begin{cases} A_{[1,3]} = A_0 = 2, & \tan\Psi_{[1,3]} = -1 = -\tan\Psi_0, \\ A_{[2,4]} = 2, & \tan\Psi_{[2,4]} = 1 = \tan\Psi_0. \end{cases}$$

The k-parameters are then given by $(k_1, k_2, k_3, k_4) = (-\frac{3}{2}, -\frac{1}{2}, \frac{1}{2}, \frac{3}{2})$. The exact solution obtained by the completion of the chord diagram is given by (3142)-type soliton solution. Figure 5.4 illustrates the result of the numerical simulation. The top figures show the direct simulation of the KP equation. We observe a bow-shape wake behind the interaction point. The wake expands and decays, and then we see the appearance of new solitons which form resonant interactions with the initial solitons. One should note that the solution generates a large amplitude intermediate soliton at the interaction point, and this soliton is identified as $[1,4]$-soliton with the amplitude $A_{[1,4]} = 4.5$. This solution has been considered to describe the Mach reflection of shallow water waves, and the $[1,4]$-soliton describes the wave called the Mach stem [3, 10].

The middle figures in Figure 5.4 show the corresponding exact solution of (3142)-type whose A-matrix is found by minimizing $E(t)$ at $t = 10$,

$$A = \begin{pmatrix} 1 & 1.92 & 0 & -1.96 \\ 0 & 0 & 1 & 0.64 \end{pmatrix}$$

In the minimization to find the A-matrix, we adjust the locations of solitons including the intermediate solitons, and using (3.5), we obtain

$$x^+_{[1,3]} = x^+_{[2,4]} = -0.01, \qquad s = 0.980.$$

Those values indicate that the solution is very close to the exact solution for all the time. The negative value of the shifts $x^+_{[i,j]}$ is due to the generation of a large amplitude soliton $[1,4]$-type (i.e. the initial solitons loose their momentum), and $s < 1$ implies that the $[1,4]$-soliton is generated after $t = 0$. Also note that the $[1,4]$-soliton now resonantly interact with $[1,3]$- and $[2,4]$-solitons to create new solitons $[1,2]$- and $[3,4]$-solitons (called the reflected waves as considered in the Mach reflection problem [11, 3, 10]). This process then seems to compensate the shifts of incident waves, even though we observe a large wake behind the interaction point. Notice that the wake disperses, and the exact solution starts to appear as the wake decays (recall again the decomposition $u_{\text{exact}} = u + v$ (where v is the wake and u is the solution).

The bottom graph in Figure 5.4 shows a rapid convergence of the initial wave to (3142)-type soliton solution with those parameters of the A-matrix and k values given above, and for the error function, we use D^t_r with $r = 12$.

5.1.4. The case (d)

The line-solitons of the initial wave are $[1,2]$-soliton in $y > 0$ and $[3,4]$-soliton in $y < 0$. This case corresponds to the solitons with a large angle interaction. For simplicity, we consider a symmetric initial data with the initial wave whose amplitudes and angles are given by

$$\begin{cases} A_{[1,2]} = A_0 = 2, & \tan\Psi_{[1,2]} = -\frac{12}{5} = -\tan\Psi_0, \\ A_{[3,4]} = 2, & \tan\Psi_{[3,4]} = \frac{12}{5} = \tan\Psi_0. \end{cases}$$

The k-parameters are then given by $(k_1, k_2, k_3, k_4) = (-\frac{11}{5}, -\frac{1}{5}, \frac{1}{5}, \frac{11}{5})$. The completion of the chord diagram gives O-type soliton solution, i.e. (2143)-type. This implies that the solution extends the initial solitons to the negative x-direction with the same types, i.e. $[1,2]$- and $[3,4]$-types in $y < 0$ and $y > 0$, respectively. One should note that the solution also generates the phase shift determined uniquely by the k-parameters. Figure 5.5 illustrates the result of the numerical simulation. The top figures show the direct simulation of the KP equation. The wake behind the interaction point has a large negative amplitude, and this corresponds to the v solution in $u_{\text{exact}} = u + v$. The middle figures show the corresponding O-type exact solution whose A-matrix is determined by minimizing the error function $E(t)$ at $t = 10$,

$$A = \begin{pmatrix} 1 & 1.91 & 0 & 0 \\ 0 & 0 & 1 & 0.17 \end{pmatrix}$$

Because of our symmetric initial data, we consider the shifts $x^+_{[1,2]} = x^+_{[3,4]}$ for the minimization, and using (3.8), we obtain

$$x^+_{[1,2]} = x^+_{[3,4]} = -0.020.$$

The negative shifts imply the slow-down of the incidence waves due to the generation of the solitons extending the initial solitons in the negative x-direction. Those new parts of solitons have the locations $x^-_{[i,j]}$. The phase shifts $\Delta x_{[i,j]} = x^-_{[i,j]} - x^+_{[i,j]}$ for the line-solitons are calculated from (3.9), and they are

$$\Delta x_{[1,2]} = \Delta x_{[3,4]} = 0.593.$$

The positivity of the phase shifts is due to the attractive force between the line-solitons, and this explains the slow-down of the initial solitons, i.e. the small negative shifts of $x^+_{[i,j]}$. The bottom graph in Figure 5.5 shows $E(t)$ which is minimized at $t = 6$, and we take $r = 12$ for the domain D^t_r. One can see a rapid convergence of the solution to the O-type exact solution with those parameters. One should however remark that for a case near the critical one with $k_2 = k_3$, there exists a large phase shift in the soliton solution, and the convergence is very slow. Note that the case

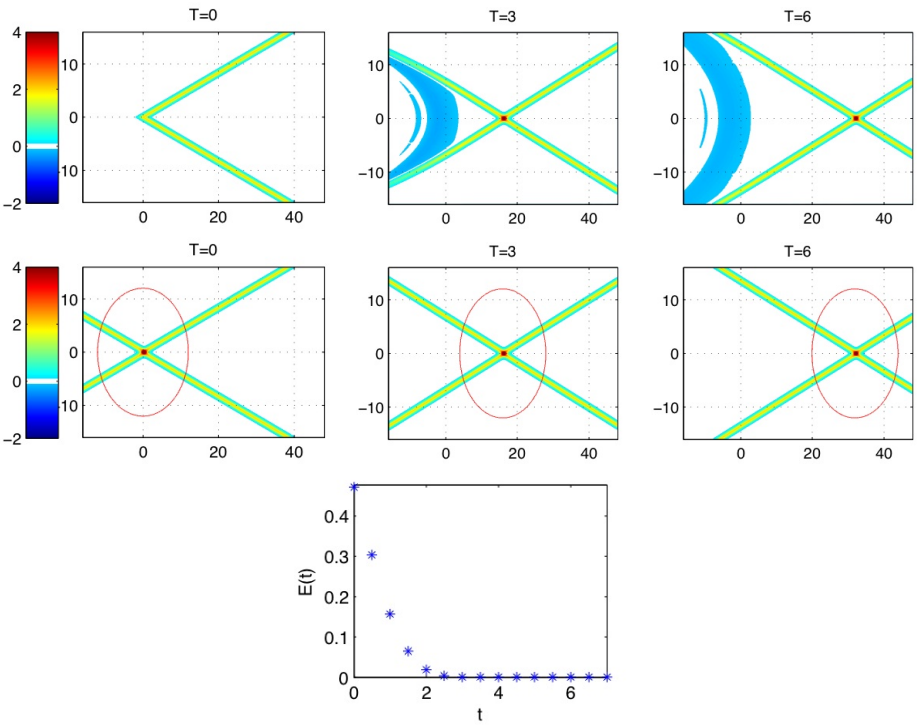

Figure 5.5: Numerical simulation of the case (d) in Figure 5.1. The initial wave consists of $[1,2]$-soliton in $y > 0$ and $[3,4]$-soliton in $y < 0$. The upper figures show the result of the direct simulation, and the middle figures show the corresponding exact solution of (2143)-type (O-type). Notice a large wake behind the interaction point which extends the initial solitons. The bottom graph shows the error function $E(t)$ which is minimized at $t = 6$.

with $k_2 = k_3$ also corresponds to the boundary of the previous case (c) (See Figure 5.1), and the amplitude of the intermediate soliton generated at the intersection point reaches *four* times larger than the initial solitons at this limit. This large amplitude wave generation has been considered as the Mach reflection problem of shallow water wave [11, 16, 3, 10, 19].

5.1.5. The case (e)

The line-solitons of the initial wave are $[2,3]$-soliton in $y > 0$ and $[1,4]$-soliton in $y < 0$. We consider the solitons parallel to the y-axis with the amplitudes,

$$\begin{cases} A_{[2,3]} = A_0 = 0.25, & \tan\Psi_{[2,3]} = 0 = -\tan\Psi_0, \\ A_{[1,4]} = 2, & \tan\Psi_{[1,4]} = 0 = \tan\Psi_0. \end{cases}$$

Then the k-parameters are given by $(k_1, k_2, k_3, k_4) = (-1, -\frac{1}{2\sqrt{2}}, \frac{1}{2\sqrt{2}}, 1)$. We also considered the case with nonzero angle (i.e. oblique to the y-axis with $\Psi_0 > 0$), and we expected to see a P-type soliton as the asymptotic solution. However, the numerical simulation suggests that we do not see a solution of P-type, but the asymptotic solution is somewhat close to the exact solution of (2341)-type as obtained by the minimal completion of the chord diagram. The (2341)-type is a $(1,3)$-type soliton solution with $[1,4]$-soliton in $y < 0$ and $[1,2]$-, $[2,3]$- and $[3,4]$-solitons in $y > 0$. Here one should note that the $[1,2]$-soliton in $y > 0$ locates ahead of the wavefront consisting of $[1,4]$- and $[2,3]$-solitons, so that this soliton cannot be generated by the resonant interaction of those $[1,4]$- and $[2,4]$-solitons.

Figure 5.6 illustrates the result of the numerical simulation. The top figures show the direct simulation of the KP equation. We observe that the $[1,4]$-soliton in $y < 0$ propagates faster and its tail extends to $y > 0$. Also note that a large dispersive wake appearing in $y < 0$ has negative amplitude and disperses in the negative x-direction. On the other hand, the tail part in $y > 0$ seems to have a resonant interaction with the $[2,3]$-initial soliton and becomes a new

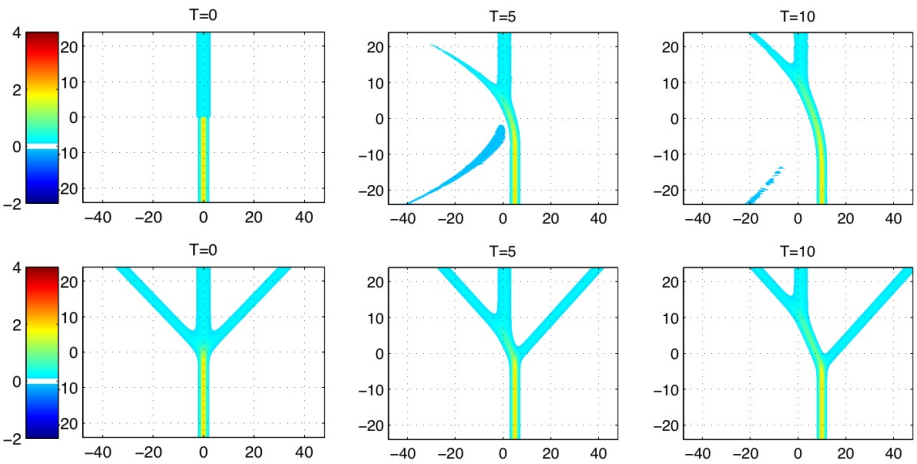

Figure 5.6: Numerical simulation of the case (e) in Figure 5.1: The initial wave consists of $[2,3]$-soliton in $y > 0$ and $[1,4]$-soliton in $y < 0$. The upper figures show the result of the direct simulation, and the lower figures show the corresponding exact solution of (2341)-type obtained by the *minimal* completion of the chord diagram given by the initial wave. Notice that the bending on the initial $[1,4]$-soliton appears near the point where the *virtual* $[1,2]$-soliton intersects. The dispersive radiation behind the intersection point may be the part of this $[1,4]$-soliton.

soliton. This behavior of the solution may be explained by the chord diagram of (2341)-type whose corresponding exact solution is illustrated in the bottom figures in Figure 5.6: The new soliton generated in $y > 0$ may be identified as $[3,4]$-soliton. Also we note that the bending of the $[1,4]$-soliton observed in the simulation seems to appear at the point where the $[1,2]$-soliton has a resonant interaction with $[1,4]$-soliton. This means that the intermediate soliton in the exact solution is $[2,4]$-soliton, and this soliton may give a good approximation of the bending part of the $[1,4]$-soliton. It is interesting to consider this $[1,2]$-soliton as a *virtual* one, which is not visible but has an influence to the initial solitons. This can be also understood by the similar argument using the decomposition $u_{\text{exact}} = u + v$. In this case, the initial data for v is given by the $[1,2]$- and $[3,4]$-solitons in u_{exact}. Then the $[3,4]$-soliton in u_{exact} appears when the solution v decays in this part. On the other hand, the decay of v in the $[1,2]$-soliton part seems to occur only in the region behind the front solitons as seen at $t = 5$. Non-decaying of the $[1,2]$-soliton implies that $[1,2]$-soliton never appears in the solution u, because of the cancellation of u_{exact} and v on this soliton part. We will give more details in a future communication.

5.1.6. The case (f)

The line-solitons of the initial wave are $[1,4]$-soliton in $y > 0$ and $[2,3]$-soliton in $y < 0$. Contrary to the previous case, we have now the larger soliton in $y > 0$ and the smaller one in $y < 0$. In a comparison, we also consider the solitons parallel to the y-axis. We then take the amplitudes and angles of the those solitons as

$$\begin{cases} A_{[1,4]} = A_0 = 6, & \tan\Psi_{[1,4]} = 0 = -\tan\Psi_0, \\ A_{[2,3]} = 2, & \tan\Psi_{[2,3]} = 0 = \tan\Psi_0. \end{cases}$$

Then the k-parameters are given by $(k_1, k_2, k_3, k_4) = (-\sqrt{3}, -1, 1, \sqrt{3})$. Since the upper $[1,4]$-soliton propagates faster than the lower one, the lower tail of this soliton appears and then resonates with the lower $[2,3]$-soliton. Following the similar arguments as in the previous case, we expect that $(3,1)$-soliton is the corresponding exact solution which is of (4123)-type as given by the minimal completion of the chord diagram. Figure 5.7 illustrates the result of the numerical simulation. The upper figures show the direct simulation, and the lower figures show the exact solution of (4123)-type. As in the previous case (e), this case shows that the $[3,4]$-soliton part in the exact solution does not appear in the solution of the simulation, that is, the $[3,4]$-soliton is a virtual one. This can be also explained with the similar argument as in the previous case. Notice again that the $[1,4]$-soliton in $y > 0$ has a virtual interaction with $[3,4]$-soliton to get bending near $(x = 18, y = 7)$ at $t = 6$.

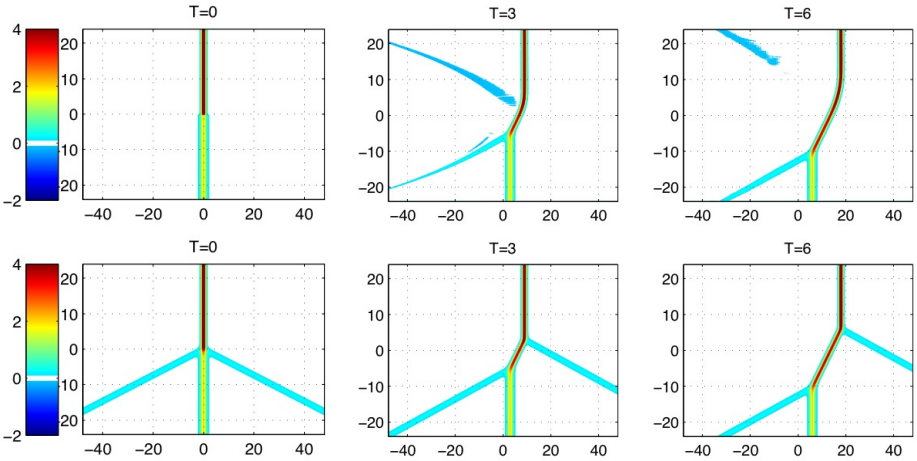

Figure 5.7: Numerical simulation of the case (f) in Figure 5.1: The initial wave consists of $[1,4]$-soliton in $y > 0$ and $[2,3]$-soliton in $y < 0$. The upper figures show the result of the direct simulation, and the lower figures show the corresponding exact solution of (4123)-type obtained by the minimal completion of the chord diagram. Notice that the bending in the $[1,4]$-soliton appears near the intersection point with the *virtual* $[3,4]$-soliton, and the dispersive radiation observed in the simulation is a part of this $[3,4]$-soliton.

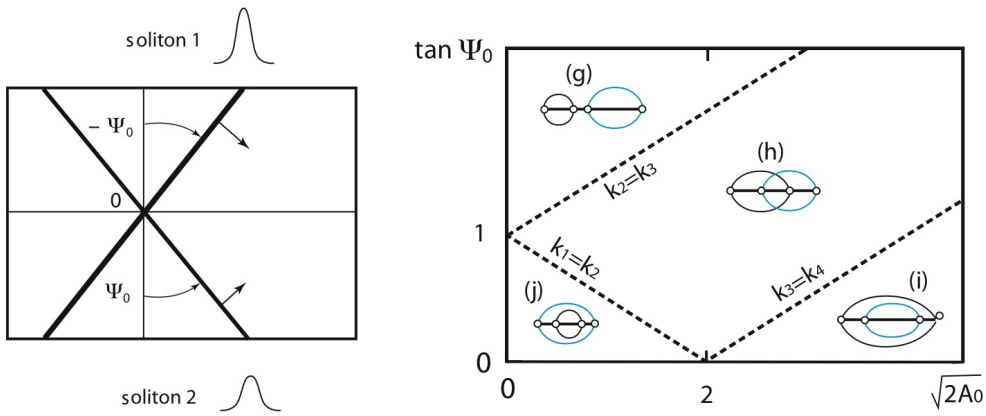

Figure 5.8: X-shape initial waves. Each line of the X-shape is an infinite line-soliton solution. We set those line-solitons to meet at the origin, and fix the amplitude of the soliton with positive angle Ψ_0 to be 2 (the corresponding chord is shown in the lighter color in each region). A_0 is the amplitude of the soliton with negative angle $-\Psi_0$. The right panel shows the corresponding chord diagrams with the choice of the values A_0 and Ψ_0. There is no exact solution for the degenerate cases marked by the dotted lines.

5.2. X-shape initial waves

The initial wave form is illustrated in the left panel of Figure 5.8. The right figure shows the chord diagrams corresponding to the initial waves with the parameters $(A_0, \tan\Psi_0)$. We carried out four different cases marked with (g) through (j) in Figure 5.8. The main result in this section is to show that each simple sum of line-solitons gets asymptotically to the exact solution corresponding to the chord diagram given by the initial wave. One should however note that those initial waves are not the exact solutions, and the simulations provide stability analysis for those exact solutions. For example, if the exact solution has the phase shift, the asymptotic solution actually converges to this exact solution by generating the correct phase shifts.

5.2.1. The case (g)

The initial wave consists of $[1,2]$- and $[3,4]$-soliton. To emphasize the phase shift appearing in the exact solution of (2143)-type, we consider the initial solitons to be close to the boundary at $k_2 = k_3$ (but we cannot take the values so close, since the generation of a large phase-shift needs a long time computation). For simplicity, we also take a

symmetric initial wave whose amplitudes and angles of the initial solitons are given by

$$\begin{cases} A_{[1,2]} = A_0 = 2, & \tan\Psi_{[1,2]} = -2.02 = -\tan\Psi_0 \\ A_{[3,4]} = 2 & \tan\Psi_{[3,4]} = 2.02 = \tan\Psi_0 \end{cases}$$

The k-parameters are then given by $(k_1, k_2, k_3, k_4) = (-2.01, -0.01, 0.01, 2.01)$. The numerical simulation in Figure 5.9 demonstrates the generation of the phase shifts after the interaction, that is, the line-solitons in the left side are accelerated by their interaction. Note here that the interaction generates the dispersive wake behind the interaction point which propagates in the negative x-direction.

Minimizing the error function $E(t)$ at $t = 12$, we obtain the A-matrix,

$$A = \begin{pmatrix} 1 & 3.029 & 0 & 0 \\ 0 & 0 & 1 & 0.015 \end{pmatrix}$$

In the minimization by adjusting the locations of the solitons, we use $x^+_{[1,2]} = x^+_{[3,4]}$ (due to the symmetry of the solution), and then we obtain

$$x^+_{[1,2]} = x^+_{[3,4]} = -0.21.$$

The negative values are due to the generation of the positive phase shifts given by (3.9),

$$\Delta x_{[1,2]} = \Delta x_{[3,4]} = 1.963 > 0.$$

Namely the accelerations of the back parts of the line-solitons (i.e. the positive phase shifts) imply the deceleration of the front parts of solitons. The middle figures in Figure 5.9 shows the corresponding O-type soliton solution with this A-matrix. The circle shows the domain D^t_r with $r = 12$. Notice the dispersive wake behind the interaction point in the simulation. The bottom graph in Figure 5.9 shows the convergence of the solution to the O-type solution given by those A-matrix and the same k-parameters.

5.2.2. The case (h)

The initial wave is the sum of $[1, 3]$- and $[2, 4]$-soliton. The corresponding chord diagram is of (3412)-type (i.e. T-type), and we expect the generation of a box at the intersection point of those solitons. For simplicity, we consider a symmetric initial wave, and take the amplitudes and angles of those solitons to be

$$\begin{cases} A_{[1,3]} = A_0 = 2, & \tan\Psi_{[1,3]} = -1 = -\tan\Psi_0 \\ A_{[2,4]} = 2 & \tan\Psi_{[2,4]} = 1 = \tan\Psi_0 \end{cases}$$

The k-parameters are then given by $(k_1, k_2, k_3, k_4) = (-\frac{3}{2}, -\frac{1}{2}, \frac{1}{2}, \frac{3}{2})$. Although T-type soliton appears for smaller angle Ψ_0, one should not take so small value. For an example of the symmetric case, if we take $\Psi_0 = 0$, we obtain the KdV 2-soliton solution with different amplitudes. So for the case with very small angle Ψ_0, we expect to see those KdV solitons near the intersection point. However, the solitons expected from the chord diagram have almost the same amplitude as the incidence solitons for the case with a small angle. The detailed study also shows that near the intersection point for T-type solution at the time when all four solitons meet at this point (i.e X-shape), the solution has a small amplitude due to the repulsive force similar to the KdV solitons (see also [4], where the initial X-shape wave with small angle generates a large soliton at the intersection point). This then implies that our initial wave given by the sum of two line-solitons creates a large dispersive perturbation at the intersection point (this can be also seen in the next cases where we discuss the P-type solutions).

The top figures in Figure 5.10 illustrate the numerical simulation, which clearly shows an opening of a resonant box as expected by the chord diagram of T-type. The corresponding exact solution is illustrated in the middle figures, where the A-matrix of the solution is obtained by minimizing the error function $E(t)$ of (5.3) at $t = 6$,

$$A = \begin{pmatrix} 1 & 0 & -0.368 & -0.330 \\ 0 & 1 & 1.198 & 0.123 \end{pmatrix}$$

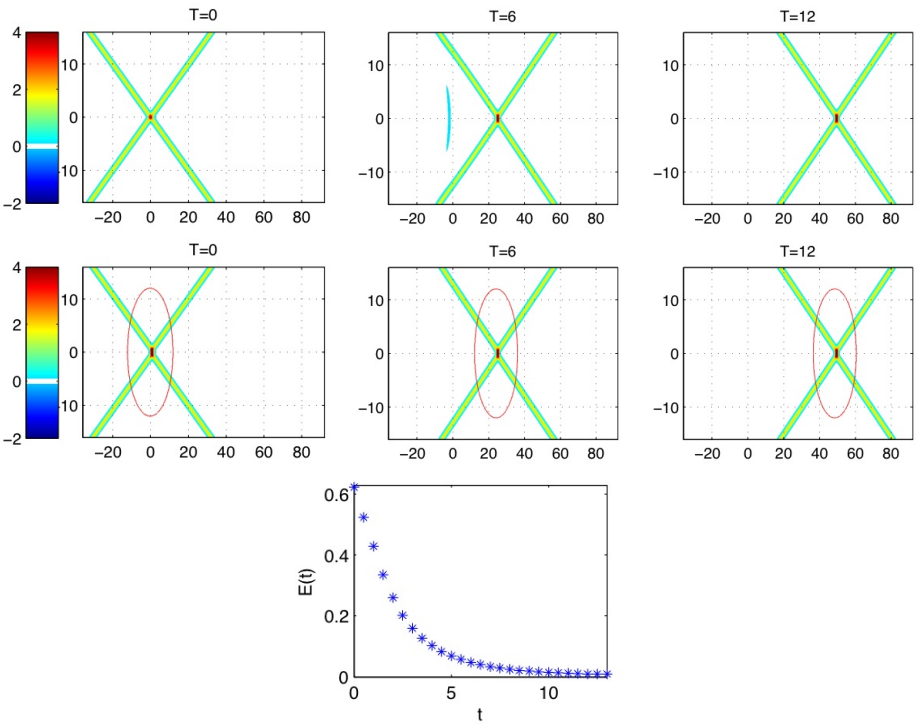

Figure 5.9: Numerical simulation of the case (g) in Figure 5.8. The initial wave is the sum of $[1,2]$- and $[3,4]$-solitons. The top figures show the numerical simulation, and the middle figures show the corresponding exact solution of (2143)-type, i.e. O-type. The bottom graph shows $E(t)$ of (5.3) which is minimized at $t = 12$. Notice that a small dispersive radiation appears to generate the correct phase shifts.

In the minimization, we take $x^{\pm}_{[1,3]} = x^{\pm}_{[2,4]}$ due to the symmetric profile of the solution, and adjust the on-set of the box (recall (3.3), and note that the symmetry reduces the number of free parameters to three). We obtain

$$x^{+}_{[1,3]} = x^{+}_{[2,4]} = 0.025, \qquad r = 3.63, \qquad s = 0.350.$$

The positive shifts of those $[1,3]$- and $[2,4]$-solitons in the wavefront indicate also the positive shift of the newly generated soliton of $[1,4]$-type at the front. This is due to the repulsive force exists in the KdV type interaction explained above, that is, the interaction part in the initial wave has a larger amplitude than that of the exact solution, so that this part of the solution moves faster than that in the exact solution. This difference may result as a shift of the location of the $[1,4]$-soliton. The phase shifts of the initial waves are obtained from (3.4),

$$\Delta x_{[1,3]} = \Delta x_{[2,4]} = 0.549.$$

The relatively large value $r > 1$ indicates that the on-set of the box is actually much earlier that $t = 0$, and $s < 1$ shows the positive phase shifts as calculated above.

The bottom graph in Figure 5.10 shows the evolution of the error function $E(t)$ of (5.3) which is minimized at $t = 6$. Note here that the circular domain D^t_r with $r = 22$ covers well the main feature of the interaction patterns for all the time computed for $t \leq 7$.

5.2.3. The case (i)

The initial wave consists of $[1,4]$- and $[2,3]$-soliton. The corresponding diagram is of (4321)-type (P-type), and the exact solution of this type has negative (repulsive) phase shift. Here we show how the phase shift is generated in the simulation. We take the amplitudes and angles of those solitons to be

$$\begin{cases} A_{[2,3]} = A_0 = \frac{8}{25}, & \tan\Psi_{[2,3]} = -0.4 = -\tan\Psi_0 \\ A_{[1,4]} = 2 & \tan\Psi_{[1,4]} = 0.4 = \tan\Psi_0 \end{cases}$$

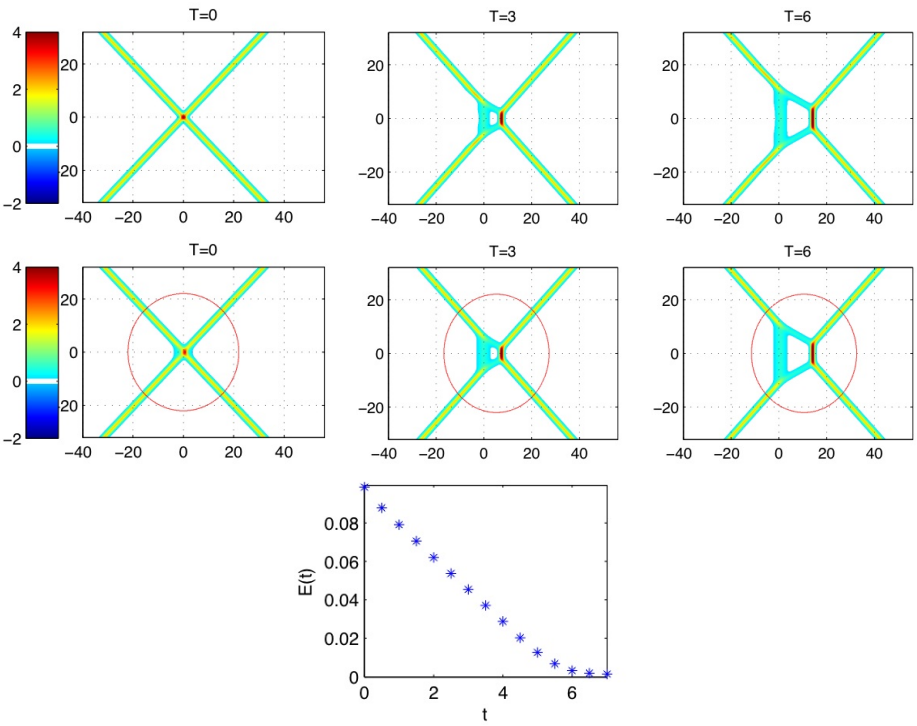

Figure 5.10: Numerical simulation of the case (h) in Figure 5.8. The initial wave is the sum of $[1,3]$- and $[2,4]$-solitons. The top figures show the numerical simulation, and the middle figures show the corresponding exact solution of (3412)-type, i.e. T-type. The bottom graph shows the error function $E(t)$ of (5.3) which is minimized at $t = 6$.

The k-parameters are then given by $(k_1, k_2, k_3, k_4) = (-\frac{4}{5}, -\frac{3}{5}, \frac{1}{5}, \frac{6}{5})$. In this case, we also note that taking a very small angle Ψ_0 may give a large perturbation to the exact solution, and one should have a large computation time to see the convergence. The top figures in Figure 5.11 show the numerical simulation. The simulation indicates the generation of the phase shift in the lower part of the solution. This may be explained as follows: Since the $[1,4]$-soliton propagates faster than the $[2,3]$-soliton, the intersection point moves in the upper direction, i.e. the positive y-direction. Then the effect of the nonlinear interaction may be observed in the lower half (i.e. behind the interactions) of the solution, and it generates the phase shifts. One should also note that the large bending of the $[1,4]$-soliton in $y < 0$. This is due to the interaction with the dispersive wake generated around the origin at $t = 0$, and notice that this bending part disperses away. The middle figures in Figure 5.11 show the corresponding exact solution of P-type whose A-matrix is obtained by minimizing the error function $E(t)$ of (5.3) at $t = 12$,

$$A = \begin{pmatrix} 1 & 0 & 0 & -0.038 \\ 0 & 1 & 1.629 & 0 \end{pmatrix}$$

In the minimization, we adjust the location of the line-solitons at the wavefront, and using (3.6), we obtain

$$x^+_{[2,3]} = -0.125, \qquad x^+_{[1,4]} = -0.54.$$

Notice that the larger shifts in the $[1,4]$-soliton, which can be also observed in the simulation. This shift is due to the repulsive force appearing at the intersection point (recall that the exact solution has a smaller amplitude at this point). The phase shifts of the P-type solution is given by (3.7),

$$\Delta x_{[1,4]} = -1.10, \qquad \Delta x_{[2,3]} = -2.75.$$

Those large phase shifts are also observed in the simulation, and the bending regions are getting separated from the intersection point with the correct phase shifts. The bottom graph in Figure 5.11 shows the decay of the error function

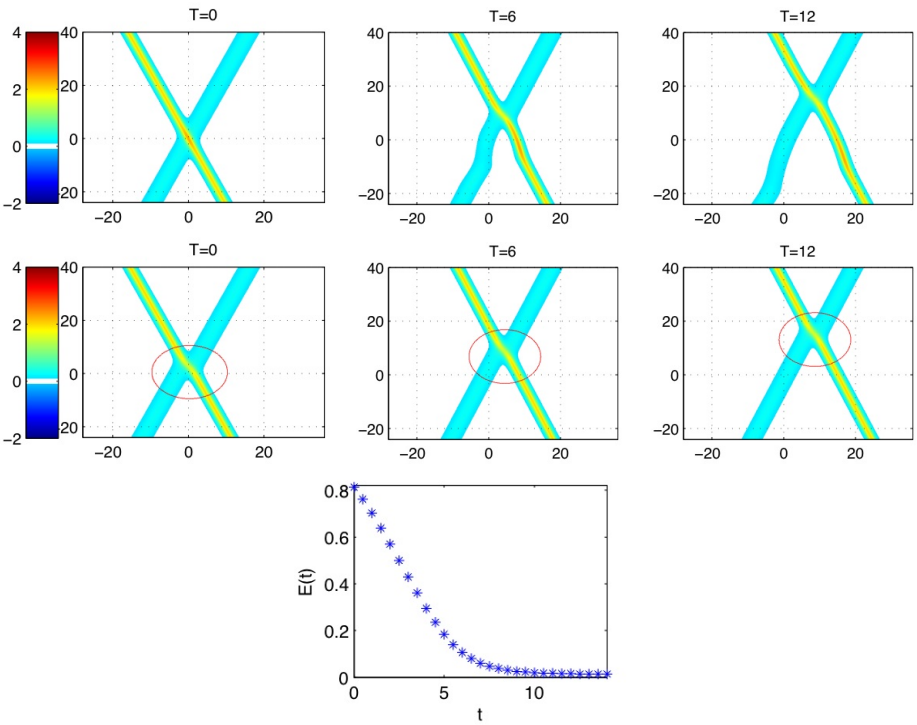

Figure 5.11: Numerical simulation of the case (i) in Figure 5.8. The initial wave is the sum of $[1,4]$- and $[2,3]$-solitons. The top figures show the numerical simulation, and the middle figures show the corresponding exact solution of (4321)-type, i.e. P-type. The bottom graph shows the error function $E(t)$ of (5.3) which is minimized at $t = 12$. Note that the bending on the solitons disperses and the interaction pattern converges locally to that of the corresponding exact solution.

$E(t)$ with D_r^t for $r = 10$. We also note the saturation $E(t)$ after $t = 11$, which may be due to the large deformation of the solution, and we may need to perform a larger domain computation.

5.2.4. The case (j)

This case is similar to the previous one with $[1,4]$- and $[2,3]$-soliton in the initial wave. However in this case, the larger soliton of $[1,4]$-type has a negative angle (propagating in the negative y-direction), and we expect that the phase shift now appear in the upper half of the solution. We take the amplitudes and angles of those solitons to be

$$\begin{cases} A_{[1,4]} = A_0 = \frac{169}{32}, & \tan\Psi_{[1,4]} = -\frac{1}{4} = -\tan\Psi_0 \\ A_{[2,3]} = 2 & \tan\Psi_{[2,3]} = \frac{1}{4} = \tan\Psi_0 \end{cases}$$

The k-parameters are then given by $(k_1, k_2, k_3, k_4) = (-\frac{7}{4}, -\frac{7}{8}, \frac{9}{8}, \frac{3}{2})$. The top figures in Figure 5.12 show the numerical simulation. One can observe a dispersive wake is generated by a large perturbation in the initial wave near the origin, and then the wake pushes the $[1,4]$-soliton forward. Also the large bending of the $[2,3]$-soliton near the origin is due to the interaction with the wake. Since the $[1,4]$-soliton propagates much faster than the other one, the intersection point moves in the negative y-direction. We can see a clear separation between the dispersive waves causing the deformation of solitons and the intersection points of P-type. The middle figures in Figure 5.12 illustrate the corresponding P-type solution whose A-matrix is obtained by minimizing the error function $E(t)$ at $t = 8$. We take the radius $r = 10$ for a good separation of the dispersive perturbation from the steady P-type soliton part. With this minimization, we get

$$A = \begin{pmatrix} 1 & 0 & 0 & -0.299 \\ 0 & 1 & 8.549 & 0 \end{pmatrix}$$

In the minimization, we adjust the locations of the line-solitons at the wavefront, and using (3.6), we obtain

$$x^+_{[1,4]} = 0.627, \qquad x^+_{[2,3]} = 0.923.$$

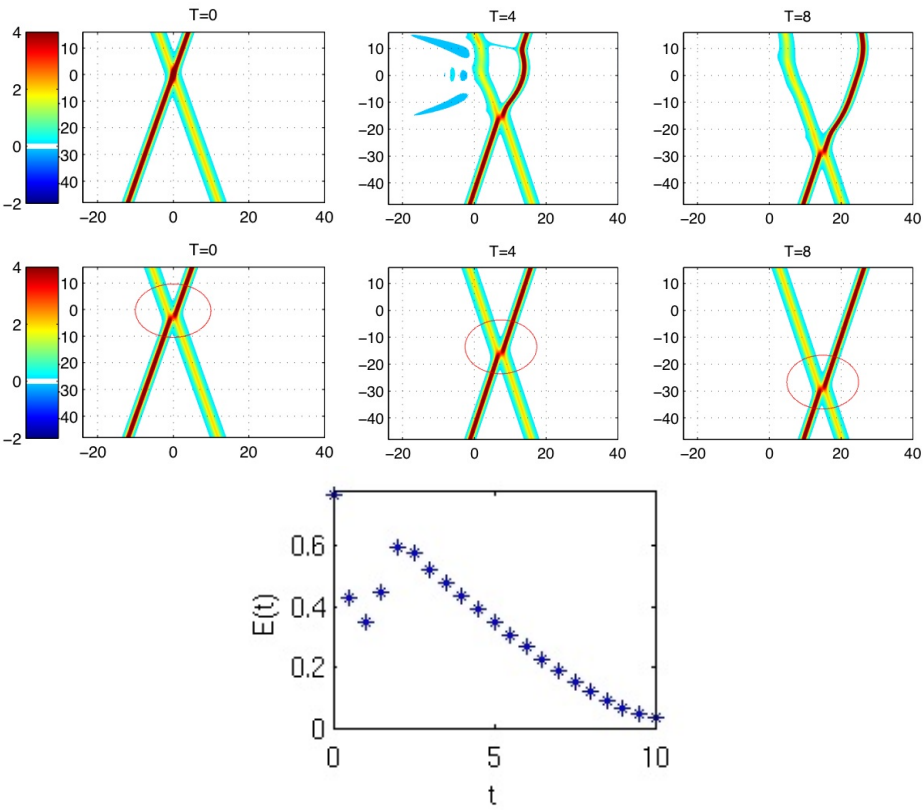

Figure 5.12: Numerical simulation of the case (j) in Figure 5.8. The initial wave is the sum of $[1,4]$- and $[2,3]$-solitons. The top figures show the numerical simulation, and the middle figures show the corresponding exact solution of (4321)-type, i.e. P-type. The bottom graph illustrates the error function $E(t)$ of (5.3) which is minimized at $t = 8$. The graph shows a further reduction of the error, that is, the convergence of the solution to the corresponding exact solution even with a drastic change of the error at the initial stage.

The positive shifts are due to the repulsive interaction at the intersection point as observed in the simulation. The phase shifts of those incidence solitons are given by (3.7),

$$\Delta x_{[1,4]} = -0.934, \qquad \Delta x_{[2,3]} = -1.518.$$

Notice that the $[1,4]$-soliton behind the $[2,3]$-soliton shifts $x^-_{[1,4]} = x^+_{[1,4]} + \Delta x_{[1,4]} = -0.307$, and it gets a larger shift in the upper part. The large bending in the simulation is generated by a strong perturbation generated at the intersection point at $t = 0$. However, the bending part disperses and the intersection point gets away from this part.

The bottom graph in Figure 5.12 shows the decay of the error. We emphasize that the error function gets a rapid change in the early times. This implies that a drastic change in the profile of the solution due to a large perturbation to the exact solution. However after $t = 3$ the solution has a monotone convergence to the exact solution, implying that the dispersive waves are getting away from the domain D^t_r as we expected.

Acknowledgement

We would like to thank Professor Thiab Taha for giving us the opportunity to present our result at the Sixth IMACS International Conference on March 23-26, 2009. We would also like to thank Professors Masayuki Oikawa, Hidekazu Tsuji and Sarvarish Chakravarty for various useful discussions related to the present work. C.-Y. K is partially supported by NSF grant DMS-0811003 and the Alfred P. Sloan fellowship. Y.K. is partially supported by NSF grant DMS-0806219.

References

[1] M. J. Ablowitz and H. Segur, *Solitons and the inverse scattering transform*, SIAM Studies in Applied Mathematics, (SIAM, Philadelphia/ 1981).

[2] S. Chakravarty and Y. Kodama, Classification of the line-solitons of KPII, *J. Phys. A: Math. Theor.*, **41** (2008) 275209 (33pp).

[3] S. Chakravarty and Y. Kodama, Soliton solutions of the KP equation and application to shallow water waves, *Stud. Appl. Math.*, **123** (2009) 83-151.

[4] M. Chen, Oblique interaction of solitary waves (preprint, 2009).

[5] M. Funakoshi, Reflection of obliquely incident solitary waves, *J. Phys. Soc. Jpn*, **49**, (1980) 2371-2379.

[6] R Hirota, *The Direct Method in Soliton Theory* (Cambridge University Press, Cambridge, 2004)

[7] B. B. Kadomtsev and V. I. Petviashvili, On the stability of solitary waves in weakly dispersive media, *Sov. Phys. - Dokl.* **15** (1970) 539-541.

[8] F. Kako and N. Yajima, Interaction of Ion-acoustic solitons in two-dimensional space, *J. Phys. Soc. Jpn*, **49** (1980) 2063-2071.

[9] Y. Kodama, Young diagrams and N-soliton solutions of the KP equation, *J. Phys. A: Math. Gen.*, **37** (2004) 11169-11190.

[10] Y. Kodama, M. Oikawa and H. Tsuji, Soliton solutions of the KP equation with V-shape initial waves, *J. Phys. A:Math. Theor.*, **42** (2009) 312001 (9pp).

[11] J. W. Miles, Resonantly interacting solitary waves, *J. Fluid Mech.*, **79** (1977) 171-179.

[12] T. Miwa and M. Jimbo and E. Date, *Solitons: differential equations, symmetries and infinite-dimensional algebras* (Cambridge University Press, Cambridge, 2000)

[13] A. C. Newell, *Solitons in Mathematics and Physics*, CBMS-NSF **48**, (SIAM, Philadelphia/ 1985).

[14] A. C. Newell and L. G. Redekopp, Breakdown of Zakharov-Shabat theory and soliton creation, *Phys. Rev. Lett.* **38** (1977) 377-380.

[15] S. Novikov, S. V. Manakov, L. P. Pitaevskii and V. E. Zakharov, *Theory of Solitons: The Inverse Scattering Method*, Contemporary Soviet Mathematics, (Consultants Bureau, New York and London, 1984).

[16] A. V. Porubov, H. Tsuji, I. L. Lavrenov and M. Oikawa, Formation of the rogue wave due to non-linear two-dimensional waves interaction, *Wave Motion* **42** (2005) 202-210.

[17] P. Schlatter, N.A. Adams and L. Kleiser, A windowing method for periodic inflow/outflow boundary treatment of non-periodic flows, *J. Comput. Phys.* **206** (2005) 505-535.

[18] H. Tsuji and M. Oikawa, Oblique interaction of solitons in an extended Kadomtsev-Petviashvili equation, *J. Phys. Soc. Japan*, **76** (2007) 84401-84408.

[19] H. Tsuji, M. Oikawa and K. Maruno, Two-dimensional interaction of long solitary waves and web solution, presented at the annual meeting of *The Japan Society of Fluid Mechanics*, Kobe, Japan, September 4-7, 2008.

[20] G. B. Whitham, *Linear and nonlinear waves*, A Wiley-interscience publication (John Wiley & Sons, New York, 1974).